Neuron

Dopamine-evoked synaptic regulation in the brain reward system requires astrocyte activity

--Manuscript Draft--

Manuscript Number:	NEURON-D-19-00828R1
Full Title:	Dopamine-evoked synaptic regulation in the brain reward system requires astrocyte activity
Article Type:	Research Article
Keywords:	Astrocytes; Dopamine; Synaptic transmission; Amphetamine
Corresponding Author:	Alfonso Araque University of Minnesota Minneapolis, MN UNITED STATES
First Author:	Michelle Corkrum
Order of Authors:	Michelle Corkrum
	Ana Covelo
	Justin Lines
	Luigi Bellochio
	Marc Pisansky
	Kelvin Loke
	Ruth Quintana
	Patrick Rothwell
	Rafael Lujan
	Giovanni Marsicano
	Eduardo D. Martin
	Mark J. Thomas
	Paulo Kofuji
	Alfonso Araque
Abstract:	Dopamine is a key neurotransmitter involved in physiological processes, such as learning and memory, motor control and reward, as well as, pathological conditions, such as Parkinson's disease and drug abuse. In contrast to the extensive studies on neurons, the role of astrocytes in dopaminergic signaling remains largely unknown. Using transgenic mice, optogenetics and pharmacogenetics, we studied the role of astrocytes on the dopaminergic system. We show that in freely-behaving mice, astrocytes in the nucleus accumbens (NAc), a key reward center in the brain, respond with Ca2+ elevations to synaptically-released dopamine, a phenomenon that is enhanced by amphetamine, a psychostimulant drug that acts via increasing dopamine levels. In brain slices, synaptically-released dopamine increases astrocyte Ca2+ and stimulates the release of ATP/adenosine, which leads to excitatory synaptic depression through activation of presynaptic adenosine A1 receptors. Amphetamine depresses neurotransmission through stimulation of astrocytes and the consequent activation of presynaptic A1 receptors. Furthermore, astrocytes modulate the acute behavioral psychomotor effects of amphetamine. Therefore, astrocytes mediate the synaptic regulation induced by dopamine and amphetamine, revealing a novel cellular pathway in the brain reward system.
Suggested Reviewers:	Frank Kirchhoff, PhD Professor, University of Saarland frank.kirchhoff@uks.eu Expert in neuron-glia interactions

	Christian Steinhausser, PhD Professor, University of Bonn christian.steinhaeuser@ukb.uni-bonn.de Expert in astrocyte information processing
	Helmut Kettenmann, PhD Professor, Max-Delbrück-Centrum für Molekulare Medizin (MDC) kettenmann@mdc-berlin.de Expert in neuron-glia interactions
	A. Jon Stoessl, MD Professor, Pacific Parkinson's Research Centre jstoessl@mail.ubc.ca Expert in dopamine signaling
	Jose Obeso, MD, PhD Professor, CINAC, Hospitales de Madrid and CEU–San Pablo University jaobeso@movementdisorders.org Expert in dopamine signaling
	Ann Graybiel, PhD MIT McGovern Institute graybiel@mit.edu Expert in dopamine signaling
	Richard Robitaille, PhD Professor, Université de Montréal richard.robitaille@umontreal.ca Expert in neuron-glia interactions
	Stéphane Oliet, PhD Professor, Université Bordeaux stephane.oliet@inserm.fr Expert in neuron-glia interactions
Opposed Reviewers:	Baljit Khakh, PhD Professor, University of California, Los Angeles bkhakh@mednet.ucla.edu Potential conflict of interest
	David Attwell, PhD Professor, University College London d.attwell@ucl.ac.uk Potential conflict of interest

DOPAMINE-EVOKED SYNAPTIC REGULATION IN THE BRAIN REWARD SYSTEM REQUIRES ASTROCYTE ACTIVITY

Michelle Corkrum[*1], Ana Covelo[*1,2,3], Justin Lines[1], Bellocchio Luigi[2,3], Marc Pisansky[1], Kelvin Loke[1], Ruth Quintana[1], Patrick Rothwell[1], Rafael Lujan [4], Marsicano Giovanni[2,3], Eduardo D. Martin[5], Mark J. Thomas[1], Paulo Kofuji[1] and Alfonso Araque[1,6#]

[*]These authors contributed equally to the work

[1] Department of Neuroscience, University of Minnesota. Minneapolis, Minnesota 55455, USA.
[2] INSERM, U1215 NeuroCentre Magendie, Bordeaux Cedex 33077, France.
[3] University of Bordeaux, Bordeaux 33000, France.
[4] Instituto de Investigación en Discapacidades Neurológicas (IDINE), Universidad Castilla-La Mancha, 02008 Albacete, Spain
[5] Instituto Cajal, CSIC, Madrid 28002, Spain.
[6] Lead contact

#Corresponding Author

Correspondence should be addressed to:
Dr. Alfonso Araque
Dept. Neuroscience
University of Minnesota
4-110 Wallin Medical Biosciences Building
2101 6th Street SE Minneapolis, MN 55455
Phone: (612) 624 0901
E-mail: araque@umn.edu

Keywords: Astrocytes, dopamine, synaptic transmission, amphetamine

SUMMARY

Dopamine is a key neurotransmitter involved in physiological processes, such as learning and memory, motor control and reward, as well as, pathological conditions, such as Parkinson's disease and drug abuse. In contrast to the extensive studies on neurons, the role of astrocytes in dopaminergic signaling remains largely unknown. Using transgenic mice, optogenetics and pharmacogenetics, we studied the role of astrocytes on the dopaminergic system. We show that in freely-behaving mice, astrocytes in the nucleus accumbens (NAc), a key reward center in the brain, respond with Ca^{2+} elevations to synaptically-released dopamine, a phenomenon that is enhanced by amphetamine, a psychostimulant drug that acts via increasing dopamine levels. In brain slices, synaptically-released dopamine increases astrocyte Ca^{2+} and stimulates the release of ATP/adenosine, which leads to excitatory synaptic depression through activation of presynaptic adenosine A_1 receptors. Amphetamine depresses neurotransmission through stimulation of astrocytes and the consequent activation of presynaptic A_1 receptors. Furthermore, astrocytes modulate the acute behavioral psychomotor effects of amphetamine. Therefore, astrocytes mediate the synaptic regulation induced by dopamine and amphetamine, revealing a novel cellular pathway in the brain reward system.

INTRODUCTION

Dopaminergic signaling plays fundamental roles in both physiologic and pathologic brain states. Dopamine is essential for movement, reward, learning and memory, and is implicated in brain disorders such as Parkinson's disease and drug addiction. The nucleus accumbens (NAc) is a key brain region in reward and addiction that receives extensive dopaminergic input from the ventral tegmental area (VTA) (Luscher, 2016; Luscher and Malenka, 2011). Dopamine depresses glutamatergic neurotransmission in the NAc (Bamford et al., 2008; Kalivas and Volkow, 2005) but the underlying mechanism remains unclear. While some reports indicate that dopamine acts on presynaptic D_1 receptors to directly depress excitatory transmission (Harvey and Lacey, 1996; Nicola et al., 1996), adenosine signaling has also been implicated in dopamine-evoked excitatory depression (Harvey and Lacey, 1997; Kombian et al., 2003; Wang et al., 2012). In contrast to the extensive studies on the function of neurons in dopaminergic signaling in the NAc, the effects of dopamine on astrocyte activity and the consequences on neurotransmission are largely unknown.

Astrocytes have traditionally been considered support cells of the brain aiding in ion homeostasis, maintaining the blood-brain barrier and providing trophic support to neurons. Accumulating data shows that astrocytes also play active roles in brain physiology being key players in the tripartite synapse (Araque et al., 1999). Astrocytes exhibit increases in intracellular Ca^{2+} in response to neurotransmitters (Araque et al., 2001; Araque et al., 2014; Di Castro et al., 2011; Haydon and Carmignoto, 2006; Navarrete and Araque, 2010; Panatier et al., 2011; Perea et al., 2016; Perea et al., 2009; Volterra et al., 2014; Volterra and Meldolesi, 2005) and, in turn, they release neuroactive substances termed gliotransmitters (Volterra and Meldolesi, 2005), that regulate synaptic transmission and plasticity (Araque et al., 2014; Bezzi et al., 2004; Covelo and Araque, 2016, 2018; Di Castro et al., 2011; Halassa and Haydon, 2010; Henneberger et al., 2010; Martin-Fernandez et al., 2017; Martin et al., 2015; Min and Nevian, 2012; Min et al., 2012; Navarrete and Araque, 2010; Panatier et al., 2011; Parri et al., 2001; Perea and Araque, 2007; Perea et al., 2016; Volterra and Meldolesi, 2005). The bidirectional signaling between neurons and astrocytes has been shown in many brain areas (Araque et al., 2014), however, the specific role of astrocytes in NAc dopamine signaling remains unknown.

Here we show that optogenetic stimulation of dopaminergic axons in freely moving animals evoke Ca^{2+} elevations in NAc astrocytes, and that these responses are altered by amphetamine. Using brain slices to identify the cellular signaling and physiological consequences, we show that astrocyte Ca^{2+} elevations evoked by synaptically-released dopamine stimulates the release of ATP/adenosine, which mediates dopamine- and amphetamine-evoked depression of excitatory transmission through activation of A_1 receptors. We also found that selective pharmacogenetic activation of astrocytes mimics the dopamine-evoked synaptic regulation. Additionally, attenuation of astrocyte Ca^{2+} signaling decreases the acute psychomotor behavioral effects of amphetamine, indicating that astrocytes are actively involved in the dopaminergic system.

RESULTS

Dopamine activates astrocyte Ca^{2+} signaling in the NAc.

Astrocytes in the globus pallidus and hippocampus (Cui et al., 2016; Jennings et al., 2017) have been shown to respond to dopamine, but whether astrocytes respond *in vivo* to synaptically-released dopamine in reward centers such as the NAc remains unknown. We

monitored astrocyte Ca^{2+} levels in the NAc using a fiber-photometry system in freely behaving mice (Lerner et al., 2015; Saunders et al., 2018) and specifically stimulated dopaminergic afferents to the NAc using optogenetics (Figures 1A and 1B). Mice expressing Cre under the dopamine transporter (DAT) promoter (DAT-IRES-Cre mice) were injected with AAV5-hSyn-FLEX-ChrimsonR-tdTomato into the VTA, to selectively express ChrimsonR (a red-shifted channelrhodopsin (Klapoetke et al., 2014)) in dopaminergic neurons projecting to the NAc (Figure 1A and Figures S1A and S1B). Mice were also injected in the NAc with AAV5-GfaABC1D-cytoGCaMP6f-SV40 to express the Ca^{2+} indicator GCaMP6f selectively in astrocytes (Figure 1A and Figure S2C). Opto-stimulation of dopaminergic axons (5ms pulses for 5 s) reliably evoked Ca^{2+} elevations in NAc astrocytes in a frequency-dependent manner (Figure 1C). These responses were absent in DAT-Cre mice injected with AAV5-GfaABC1D-GFP in the NAc (i.e., lacking GCamp6f) and in DAT-Cre WT (Cre -negative mice) injected with a hSyn-FLEX-ChrimsonR-TdTomato in the VTA (Figure 1D), indicating that they were not artifacts due to optogenetic stimulation, and they were abolished by flupenthixol (5mg/kg), confirming that the recorded signal was evoked by dopamine (Figure 1D). Moreover, the amplitude, rise time and width of the dopamine-evoked astrocyte Ca^{2+} responses were augmented by amphetamine (2.5 mg/kg) (n = 19 responses in control and n = 19 responses in amphetamine from n = 5 animals; Figures 1E and 1F), which is consistent with its known mode of action to increase synaptic dopamine (Calipari and Ferris, 2013). Taken together, these *in vivo* results indicate that NAc astrocytes respond with Ca^{2+} elevations to dopamine released by synaptic terminals from the VTA, and that these responses are regulated by amphetamine.

Ultrastructural results from electron microscopy experiments indicate that D_1 receptors (D_1Rs) localize not only at the axon terminals and in the postsynaptic terminals, but also in astrocytes (Figure 1G), suggesting that astrocytes are able to sense dopamine and that the recorded responses could result from direct activation of astrocytes by dopamine.

To test this idea, we used brain slices to examine astrocyte responsiveness to dopamine. Local application of dopamine from a micropipette (500 μM, 5 s, 0.5 bar) in the presence of TTX (1 μM) elevated Ca^{2+} in 47 out of 75 astrocytes (n = 7). Dopamine stimulation of astrocytes, manifested as increased Ca^{2+} activity, quantified as Ca^{2+} event probability (Covelo and Araque, 2018; Gomez-Gonzalo et al., 2015; Martin-Fernandez et al., 2017; Martin et al., 2015; Navarrete and Araque, 2010; Perea et al., 2016), occurred in both somas (from 0.14 ± 0.05

to 0.63 ± 0.07, n = 7 slices, Figure 2A and 2B) and processes (from 0.19 ± 0.04 to 0.54 ± 0.07, n = 7 slices, Figure 2A and 2B). Astrocyte responsiveness to dopamine remained in the presence of a cocktail of neurotransmitter receptor antagonists (CNQX 20 μM, AP5 50 μM, MPEP 50 μM, LY367385 100 μM, picrotoxin 50 μM, CGP5462 1 μM, atropine 50 μM, CPT 10 μM, and suramin 100 μM) that also contained TTX (1 μM; Figure 2B), suggesting that dopamine acts on NAc astrocytes to elevate Ca^{2+} levels. While these results suggest that the dopamine-evoked Ca^{2+} responses were mediated by direct activation of astrocytes, an indirect effect mediated by a neuronal signal cannot be totally ruled out. However, a more specific approach of deleting D_1 receptors only in astrocytes using the GFAP-$D_1^{-/-}$ mice further indicates that dopamine-evoked Ca^{2+} responses were mediated by direct activation of astrocytic D_1 receptors (see below, Figure 4C and 4D). We then investigated astrocyte responsiveness to synaptically released dopamine using the optogenetic approach described above in the presence of the cocktail of neurotransmitter receptor antagonists without TTX. Optogenetic stimulation of dopaminergic axons (5 ms pulses for 5 s at 30 Hz) elevated astrocyte Ca^{2+} in 39 out of 110 astrocytes, in both somas (from 0.11 ± 0.04 to 0.37 ± 0.06, n = 14 slices) and processes (from 0.19 ± 0.03 to 0.40 ± 0.03, n = 6 slices) in mice expressing ChrimsonR (Figures 2C and 2D), but not in control mice (Cre negative, i.e., wild-type DAT littermate mice lacking Cre injected with AAV5-hSyn-FLEX-ChrimsonR-tdTomato; n = 5; Figure 2D). Consistent with results found *in vivo*, astrocyte responses to opto-stimulation was frequency-dependent (Figure S1C).

The astrocyte Ca^{2+} responses to dopamine were abolished by the broad dopamine receptor antagonist flupenthixol (30 μM; n = 125 astrocytes from n = 11 slices for applied dopamine; n = 143 astrocytes from n = 12 slices for opto-stimulation; Figures 2B and 2D), and by the D_1 receptor antagonist SCH 23390 (5 μM; n = 62 astrocytes from n = 4 slices for applied dopamine; n = 121 astrocytes from n = 6 slices for opto-stimulation; Figures 2B and 2D), but unaffected by the D_2 receptor antagonist sulpiride (10 μM; n = 189 astrocytes from n = 14 slices for applied dopamine; n = 222 astrocytes from n = 13 slices for opto-stimulation; Figures 2B and 2D). Taken together and consistent with ultrastructural evidence, these results indicate that NAc astrocytes express D_1 receptors and respond with Ca^{2+} elevations to synaptically-released dopamine through activation of D_1Rs.

Dopamine-evoked excitatory synaptic regulation is mediated by astrocytes

We next investigated the consequences of the dopamine-induced astrocyte Ca^{2+} elevations on excitatory synaptic transmission in the NAc. We recorded excitatory postsynaptic currents (EPSCs) from medium spiny neurons (MSNs) before, during and after local application of dopamine while monitoring astrocyte Ca^{2+} levels (Figure 3A). Local application of dopamine, which increased astrocytic Ca^{2+}, transiently depressed EPSC amplitude (from 97.6 ± 2.3 to 74.6 ± 6.2%, n = 9; Figures 3A and 3C and Figures S3A-S3D) (Harvey and Lacey, 1996; Nicola et al., 1996). Likewise, synaptically-released dopamine increased astrocytic Ca^{2+} and depressed EPSCs in mice that expressed ChrimsonR (from 98.3 ± 2.6 to 75.6 ± 2%, n = 13; Figures 3B and 3E and Figures S3E-S3H) but not in Cre negative mice (n = 6; Figure S3H). The dopamine-induced EPSC depression was associated with an enhancement of the paired pulse ratio (PPR) (from 1.1 ± 0.05 to 1.4 ± 0.07, n = 15, for applied dopamine; from 1.04 ± 0.08 to 1.32 ± 0.14, n = 11; for opto-stimulation Figures S3C and S3G), suggesting a presynaptic mechanism. For both applied and synaptic dopamine there was a correlation between astrocyte Ca^{2+} elevation changes and percentage of EPSC depression (r^2 = 0. 361, n = 19 and r^2 = 0.6214, n = 11 for applied dopamine and opto-stimulation, respectively; Figures 3D and 3F). Consistent with the effects on astrocyte Ca^{2+}, the synaptic effects were abolished by flupenthixol (n = 6 and n = 4 for applied dopamine and opto-stimulation, respectively; Figures S3D and S3H) and by SCH 23390 (n = 9 and n = 6 for applied dopamine and opto-stimulation, respectively; Figures S3D and S3H), but unaffected by sulpiride (n = 8 and n = 6 for applied dopamine and opto-stimulation, respectively; Figures S3D and S3H). These results indicate that dopamine acts via D_1-like receptors to presynaptically depress excitatory synaptic transmission (Harvey and Lacey, 1996; Nicola et al., 1996), and that this synaptic regulation is associated with astrocyte Ca^{2+} elevations.

Next, we tested whether the astrocyte activity was necessary for the dopaminergic modulation of excitatory synaptic transmission. We used $IP_3R2^{-/-}$ mice (Li et al., 2005), in which G protein-mediated Ca^{2+} elevations are largely impaired in astrocytes (Gomez-Gonzalo et al., 2017; Gomez-Gonzalo et al., 2015; Martin et al., 2015; Petravicz et al., 2008). In slices from these mice, astrocyte Ca^{2+} levels and synaptic transmission were both unaffected by dopamine (Ca^{2+}: n = 135 astrocytes from n = 15 slices; EPSC: n = 8; Figure 4B), suggesting that the dopamine-evoked synaptic regulation requires astrocyte activation manifested by the Ca^{2+} signaling. To further test this hypothesis, we selectively ablated G protein signaling in astrocytes by injecting astrocytes through a whole-cell recording pipette with GDPßS (10 mM) (Navarrete

and Araque, 2010; Navarrete et al., 2012), a GDP analog that competitively inhibits GTP binding to G proteins and prevents the activation of G protein signaling cascades. In MSNs located within the region of the GDPßS-loaded astrocyte network (Figure 4A), dopamine did not affect astrocyte Ca^{2+} levels (n = 45 astrocytes from n = 4 slices; Figure 4B) or EPSCs (n = 6; Figure 4B). Taken together, these results indicate that activation of G protein signaling in astrocytes is necessary for dopaminergic depression of EPSCs in the NAc.

D_1 receptors specifically expressed in astrocytes mediate dopamine-evoked depression of synaptic transmission

To specifically examine the contribution of astrocyte D_1 receptors in the NAc, we selectively deleted astroglial D_1 receptors in the NAc, by injecting mice containing the D_1 receptor gene floxed (DRD1 flox/flox mice) with AAV8-GFAP-mCherry-Cre into the NAc (GFAP-$D_1^{-/-}$ mice; Figure 4C and Figures S4A and S4B). As controls, virus-injected wild-type littermate mice (i.e., non-floxed DRD1mice; GFAP-D_1^{WT}) were used. To test the cell specificity of our approach, we examined neuronal sensitivity to D_1 signaling. Cd^{2+}-sensitive neuronal voltage-gated Ca^{2+} currents were depressed by the D_1 agonist SKF 38393 (Surmeier et al., 1995) in both GFAP-D_1^{WT} mice and GFAP-$D_1^{-/-}$ mice (Figures S4C-S4F), indicating that neuronal sensitivity to D_1 signaling remained intact in GFAP-$D_1^{-/-}$ mice.

We next investigated astrocyte responsiveness to dopamine and dopamine-evoked synaptic regulation in GFAP-$D_1^{-/-}$ mice. Dopamine elevated Ca^{2+} in astrocytes from GFAP-D_1^{WT} mice (n = 136 astrocytes, n = 5 slices; Figure 4D) but not from GFAP-$D_1^{-/-}$ mice (n = 88 astrocytes, n = 9 slices; Figure 4D). In contrast, astrocytes from both GFAP-D_1^{WT} (n = 133 astrocytes, n = 10 slices; Figure 4D) and GFAP-$D_1^{-/-}$ mice responded to ATP (n = 222 astrocytes from n = 6; Figure 4D), indicating that the astrocyte Ca^{2+} machinery was preserved. We observed an elevated basal Ca^{2+} event probability in GFAP-$D_1^{-/-}$ mice when compared to GFAP-D_1^{WT} mice (p=0.006; Table S3) suggesting that tonic D_1 receptor activation regulate basal Ca^{2+} signaling in astrocytes. In addition, the dopamine-evoked synaptic regulation was also absent in GFAP-$D_1^{-/-}$ mice (n = 8; Figure 4E), while remaining present in GFAP-D_1^{WT} mice (n = 8; Figure 4E). These results indicate that D_1 receptors specifically expressed in astrocytes mediate the dopamine-evoked depression of EPSCs in the NAc.

Astrocytes mediate synaptic depression via ATP/Adenosine signaling

Adenosine has been proposed to mediate the dopamine-induced synaptic depression in the NAc (Harvey and Lacey, 1997; Kombian et al., 2003; Wang et al., 2012), but the source of adenosine remains unknown. Astrocytes can release different gliotransmitters (Araque et al., 2014), including ATP and its metabolic product adenosine, that regulate synaptic transmission in several brain areas (Martin et al., 2007; Panatier et al., 2011; Pascual et al., 2005; Serrano et al., 2006; Zhang et al., 2003). Therefore, we hypothesized that ATP/adenosine is the gliotransmitter that mediates the dopamine-induced synaptic regulation. Dopamine-evoked synaptic depression was prevented by the adenosine A_1 receptor antagonist CPT (2 µM; n = 7 and n = 7 for applied dopamine and opto-stimulation, respectively; Figures 5A and 5B), without affecting the astrocyte Ca^{2+} (n = 85 astrocytes from n = 6 slices and n = 60 astrocytes from n = 5 slices for applied dopamine and opto-stimulation, respectively; Figures 5A and 5B). Moreover, exogenous adenosine application (250 µM, 5 s, 0.5 bar) evoked a similar neurotransmission depression as dopamine (n = 6 and n = 6, respectively; Figures 5D and 5E), confirming that A_1 receptors mediate depression of EPSCs. Notably in GDPßS-loaded astrocyte network and in $IP_3R2^{-/-}$ mice, although dopamine was unable to depress excitatory transmission, adenosine depressed the neurotransmission (Figures 5C-5E), indicating that adenosine acts downstream of the astrocyte Ca^{2+} signal. Taken together, these results indicate that dopamine-evoked synaptic depression is mediated by activation of astrocytes, and suggest sequential mechanisms that involve astrocytic D_1R activation, astrocyte Ca^{2+} elevations, ATP/adenosine release and activation of presynaptic A_1 receptors (Figure 5F).

Astrocyte Ca^{2+} elevations are sufficient to depress excitatory transmission in the NAc

To further test the involvement of astrocytes in synaptic depression regulation, we investigated if activation of G protein-mediated signaling in astrocytes was sufficient to depress excitatory transmission in the NAc by directly and selectively activating astrocytes using designer receptors exclusively activated by designer drugs (DREADDs). We targeted astrocytes in the NAc with AAV8-GFAP-Gq-DREADD-mCherry (Figure 6A and Figures S5A-S5C). Activation of Gq-DREADD expressing astrocytes with clozapine-N-oxide (CNO) induced both astrocyte Ca^{2+} elevations (n = 43 astrocytes from n = 8 slices; Figures 6B) and EPSC depression (n = 10; Figures 6C), resulting in an increase in PPR (n = 10; Figure S5D), indicating a presynaptic mechanism. Furthermore, the DREADD-mediated synaptic regulation was prevented by CPT (n = 7; Figure 6C), while the astrocyte Ca^{2+} elevations remained unaffected (n = 32

astrocytes from n = 5 slices; Figure 6B). No changes in astrocytic Ca^{2+} (n = 46 astrocytes from n = 6 slices) or synaptic transmission (n = 6) were observed in response to CNO in slices from control AAV8-GFAP-mCherry injected animals (Figure 6B and 6C). Taken together, these results indicate that astrocyte activation depresses excitatory transmission in the NAc via A_1 receptor signaling.

The psychostimulant amphetamine modulates excitatory synaptic transmission through activation of astrocytes

The results above indicate that astrocytes are key elements in dopaminergic signaling in the NAc. We then investigated the effects of amphetamine on astrocyte Ca^{2+} signaling and synaptic transmission. Amphetamine (10 µM) increased the Ca^{2+}-oscillation frequency in astrocytes (n = 32 astrocytes from n = 6 slices; Figures 7A-7D) and depressed EPSCs (n = 5; Figures 7E-7G). Both effects were blocked by flupenthixol (for Ca^{2+}: n = 34 astrocytes from n = 5 slices, Figure 7D; for EPSCs: n = 5, Figure 7G), indicating the involvement of dopamine receptors. We then tested whether astrocyte activation was necessary for amphetamine actions on EPSCs. We utilized three complementary approaches and found that in slices with GDPßS-loaded astrocytes, and in slices from $IP_3R2^{-/-}$ mice and from GFAP-$D_1^{-/-}$ mice, amphetamine-induced astrocyte Ca^{2+} elevations were absent (n = 66 astrocytes, n = 5 slices; n = 96 astrocytes, n = 9 slices; n = 119 astrocytes, n = 11 slices, respectively; Figure 7D) and amphetamine-evoked depression of EPSCs was no longer present (n = 6, n = 6, and n = 5, respectively; Figure 7G). Moreover, amphetamine-induced synaptic depression was abolished by the adenosine A_1 receptor antagonist CPT (n = 7; Figure 7G), without affecting Ca^{2+} elevations in astrocytes (n = 109 astrocytes from n = 9, Figure 7D). Taken together, these results indicate that amphetamine acts via the activation of astrocyte D_1Rs and G protein signaling, and the subsequent release of ATP/adenosine to depress excitatory synaptic transmission.

Next, we investigated the role of astrocytes on the acute behavioral psychomotor effects of amphetamine. We found that the locomotion enhancement evoked by amphetamine was significantly reduced in $IP_3R2^{-/-}$ mice and GFAP-$D_1^{-/-}$ mice when compared to wild-type controls (Figures 7H and 7I). These results indicate that mice with astrocytes with impaired responses to dopamine also have decreased sensitivity to amphetamine, suggesting that astrocytes contribute to the acute psychomotor behavioral effects of amphetamine.

DISCUSSION

Present results show that astrocytes in the NAc core, a key brain region involved in reward and addiction, respond to synaptically-released dopamine *in vivo* and in slices with Ca^{2+} increases mediated by activation of D_1 receptors, which are expressed by astrocytes as evidenced by electronmicroscopy. Furthermore, dopamine, amphetamine and DREADD activation of astrocytes stimulate the release of ATP/adenosine, which activates neuronal presynaptic A_1 receptors and depresses excitatory synaptic transmission. These results indicate that NAc astrocytes are key elements of the dopaminergic system in a brain reward circuit.

In addition to passive support roles, astrocytes have been shown to play crucial roles in mediating synaptic transmission and plasticity in various brain regions such as hippocampus, cortex, amygdala and dorsal striatum (Covelo and Araque, 2018; Martin-Fernandez et al., 2017; Martin et al., 2007; Panatier et al., 2011; Pascual et al., 2005). Present findings reveal a key role of astrocytes in the NAc. The astrocyte responsiveness to dopamine through activation of D_1 receptors agrees with previous reports showing that astrocytes respond to dopamine with Ca^{2+} increases in the hippocampus and globus pallidus (Cui et al., 2016; Jennings et al., 2017), and contrasts with a report that failed to detect Ca^{2+} changes in response to the D_1 receptor agonist SKF 38393 in the NAc (D'Ascenzo et al., 2007).

Astrocytes in the basal ganglia have been suggested to be able to express a variety of dopamine receptors, including D_5 receptors (Brito et al., 2004; Miyazaki et al., 2004). Our results obtained with a genetic approach indicate that the dopamine-evoked astrocyte Ca^{2+} responses are selectively mediated by D_1 receptors. Nevertheless, a potential partial involvement of D_5 receptors, undetected in our experimental conditions, cannot be totally excluded. Likewise, D_2-like receptors in astrocytes have been shown to regulate basal intracellular Ca^{2+} levels in astrocytes in hippocampus and globus pallidus (Cui et al., 2016; Jennings et al., 2017). However, our results indicate that D_2-like receptors do not contribute to the dopamine- or amphetamine-evoked astrocyte Ca^{2+} responses and synaptic regulation in the NAc. Perhaps, astrocytes in different brain regions may express different dopamine receptors in different brain regions, or different dopamine receptors serve distinct brain area-specific signaling.

Present results indicate that D_1-evoked Ca^{2+} increases in astrocytes were mediated by IP_3 signaling, which contrasts with the classical view that D_1-like receptors are coupled to G_s proteins and cAMP production (Beaulieu and Gainetdinov, 2011), but which is consistent with

studies showing that D_1-like receptors can also lead to phospholipase C (PLC) activation and intracellular Ca^{2+} increases in an IP_3-dependent manner in cultured neurons (Jin et al., 2003; Lezcano and Bergson, 2002; Tang and Bezprozvanny, 2004) and astrocytes (Zhang et al., 2009), as well as in brain slices (Medvedev et al., 2013). Present results also show that this IP_3-dependent signaling cascade is involved in ATP/adenosine release from astrocytes and mediates both the dopamine synaptic regulation, a phenomenon independent of cAMP levels (Harvey and Lacey, 1997; Nicola et al., 1996), and the amphetamine effects on synaptic transmission and locomotion. Moreover, these results are also consistent with previous reports showing that D_1 receptors activation stimulates PLC and IP_3 production in the striatum in response to amphetamine, cocaine or apomorphine (Medvedev et al., 2013).

Interestingly, our data shows differences in the effectiveness to induce astrocyte responses by exogenously applied or synaptically-released dopamine (63% and 35% of responding astrocytes, respectively). These differences could be accounted for by the different experimental approaches; indeed, exogenous DA application may be more effective in targeting more astrocytes than optogenetic stimulation of dopaminergic afferents. An alternative explanation for this observation could be that different subpopulations of astrocytes with different ability to respond to dopamine may exist in the NAc. Further studies, out of the scope of the present work, are required to investigate this exciting question.

Dopamine is known to depress excitatory transmission in the NAc (Bamford et al., 2008; Kalivas and Volkow, 2005), however, the exact mechanism of dopamine-evoked depression was unclear. While some studies proposed a direct activation of D_1 receptors located in excitatory presynaptic terminals (Harvey and Lacey, 1996; Nicola et al., 1996); (Nicola and Malenka, 1997), other studies suggested the intermediate signaling molecule ATP/adenosine to mediate dopamine effects in the NAc (Harvey and Lacey, 1997; Kombian et al., 2003; Wang et al., 2012), although the exact source of ATP/adenosine remained unknown. The present results show that dopamine-evoked depression of excitatory synaptic transmission in the NAc is mainly mediated by astrocytic D_1 receptors. This is based on the following observations: i) astrocytes express D_1 receptors; ii) astrocytes respond *in vivo* and *in slices* to synaptically-released dopamine with Ca^{2+} elevations mediated by activation of D_1 receptors; iii) dopamine-evoked synaptic depression was absent when astrocyte activation was blocked by GDPβS-loading and in $IP_3R2^{-/-}$ mice; iii) dopamine-evoked synaptic depression was absent in the GFAP-$D_1^{-/-}$ mice that

lacked D_1 receptors specifically in astrocytes. In addition, the present results show that selective activation of DREADD-expressing astrocytes depresses synaptic transmission through an A_1 receptor-mediated mechanism. Taken together these results indicate that astrocytes release ATP/adenosine downstream of the Ca^{2+} signal. Based on these findings, and reconciling previous apparent contradictory reports, we propose the following mechanistic interpretation of the results: synaptically-released dopamine activates D_1 receptors in astrocytes, increasing their intracellular Ca^{2+} and stimulating the release of ATP/adenosine, which acting on presynaptic A_1 receptors depress excitatory synaptic transmission.

Dopamine regulates excitatory and inhibitory synaptic transmission, plasticity and neuronal excitability through an extensive number of cellular mechanisms that may not be mutually exclusive (Nicola and Malenka, 1997; Nicola et al., 2000; Tritsch and Sabatini, 2012). Present study reveals a novel mechanism on synaptic regulation by dopamine and amphetamine in which astrocytes and gliotransmission play a critical role. This novel mechanism does not necessarily exclude the existence of other mechanisms underlying synaptic effects of dopamine and amphetamine, such as the regulation of presynaptic conductance (Nicola and Malenka, 1997), modulation of postsynaptic firing (Nicola et al., 2000), or NMDA-dependent long-term synaptic depression (Lüscher and Malenka, 2011). The additional mechanism provided by astrocytes adds further complexity to the diverse synaptic regulatory phenomena underlying reward and addiction

Astrocytes in the NAc have been proposed to regulate neuronal excitability and addiction through the astrocytic release of glutamate in response to mGluR5 stimulation or to acute activation with DREADDs (D'Ascenzo et al., 2007; Scofield et al., 2015). While in brain areas such as cortex, hippocampus or dorsal striatum, astrocytic glutamate has been shown to regulate neurotransmission (see Araque et al., 2014), our results indicate that the regulation of synaptic transmission in the NAc evoked by dopamine and acute activation with DREADDs is mediated by astrocytic ATP/adenosine signaling, which has also been shown to modulate neurotransmission in other brain regions such as retina, cortex, hippocampal CA1, dentate gyrus and amygdala (Newman, 2003; Martín et al., 2007; Halassa et al., 2009; Di Castro et al., 2011; Panatier et al., 2011; Martin-Fernandez et al., 2017). Although our proposed mechanism for dopamine-evoked synaptic depression involves ATP/adenosine released from astrocytes, it does not necessarily exclude the existence of other gliotransmitters, such as glutamate, which has been

shown to be released by NAc astrocytes (Scofield et al., 2015). We have recently reported that single hippocampal astrocytes can release distinct gliotransmitters in response to different neuronal stimuli (Covelo and Araque, 2018). Hence, it is possible that NAc astrocytes may release both gliotransmitters depending on the input signal received and with different regulatory consequences. Further studies are required to test the possible interaction between glutamate and adenosine release from astrocytes and its physiological consequences in the NAc.

Astrocytes have been proposed to be involved in drug seeking behavior (Scofield et al., 2015), but the synaptic mechanism of action has not been completely elucidated. Present results show that astrocytes respond to synaptically-released dopamine and consequently regulate excitatory neurotransmission through the release of ATP/adenosine and activation of neuronal A_1 adenosine receptors. In addition, they also show that astrocytes are in part responsible for the synaptic effects of the psychostimulant amphetamine. Additionally, the present study shows the first evidence of astrocyte responsiveness to dopamine and amphetamine in freely behaving mice. Our results show that astrocytes are key elements in dopaminergic signaling in the NAc, are modulated by amphetamine and mediate its actions, indicating that they play critical roles in the synaptic regulation in the reward system. Elucidating the cellular mechanisms involved in dopamine neuromodulation is essential for developing efficacious therapies for diseases involving disrupted dopaminergic transmission such as Parkinson's disease and drug addiction. Hence, astrocytes may be potential novel cellular targets for treatment of neuropsychiatric disorders associated with disrupted dopaminergic signaling, such as motivation disorders and drug addiction.

ACKNOWLEDGEMENTS

We thank D. Deters and S. Jamison for technical assistance and members of the Thomas lab and Araque lab for helpful suggestions. We thank E. Larson and the MnDRIVE Optogenetics Core at the University of Minnesota for academic, technical support and acquisition of fiber photometry system. We thank T. Nichols-Meade and M. Benneyworth at the Mouse Behavior Core, University of Minnesota for academic and technical support. Work was done using Leica SP5 multi-photon microscope at the University of Minnesota - University Imaging Centers. We thank the University of Minnesota Viral Vector and Cloning Core for production of some of the viral vectors used in this study. This work was supported by NIH-NIDA (1F30DA042510-01) to M.C., Salvador de Madariaga Program (Spain) to E.D.M. and NIH-NINDS (R01NS097312-01),

Human Frontier Science Program (Research Grant RGP0036/2014) and NIH-NIDA (R01DA048822) to A.A.

AUTHOR CONTRIBUTIONS

M.C. and A.C. performed the experiments and analyzed the data. J.L. created custom MATLAB script for fiber photometry data analysis. M.P. and P.R. contributed expertise for fiber photometry experiments. L.B. and G.M. contributed to behavior experiments. E.D.M contributed expertise for *in vivo* experiments. R.Q. and P. K performed immunohistochemistry. K.L. conducted stereotaxic surgeries. R. L. performed electron microscopy. M. J. T. aided in planning and interpreting experiments. M.C., A.C. and A.A. conceived the study and wrote the manuscript. All the authors read and edited the manuscript.

DECLARATION OF INTERESTS

The authors declare no competing financial interests.

STAR METHODS

Ethics Statement: All animal care and sacrifice procedures were approved by the University of Minnesota Institutional Animal Care and Use Committee (IACUC) with compliance to the National Institutes of Health guidelines for the care and use of laboratory animals.

Animals: Mice were housed under 12/12-h light/dark cycle and up to five animals per cage. The following animals (males and females) were used for the present study C57BL/6J, $IP_3R2^{-/-}$ (generously donated by Dr. J. Chen), DrD1 flox/flox (Drd1tm2.1Stl; JAX #025700), DAT-IRES-Cre, GLAST-GCaMP3 (generously donated by Dr. D. Bergles and Dr A. Agarwal). Young (p15-p21) and adult (≥ 4 weeks) mice were used. GLAST-GCaMP3 mice were generated by crossing R26-lsl-GCaMP3 mice (JAX #014538) (Paukert et al., 2014) with the GLAST-CreERT2 mice (MGI:3830051)(Mori et al., 2006). As CreERT2 protein is inactive in the absence of tamoxifen treatment, expression of GCaMP3 was obtained in adult mice (8 weeks) by 8 daily injections of tamoxifen (1 mg, i.p.), dissolved in 90% sunflower oil, 10% ethanol to a final concentration of 10 mg/ml. The animals were used ≥ 2 weeks after tamoxifen treatment.

Slice Preparation: Animals were rapidly decapitated and the brain was placed in ice-cold artificial cerebral spinal fluid (ACSF). ACSF contained (in mM): NaCl 124, KCl 2.69, KH_2PO_4 1.25, $MgSO_4$ 2, $NaHCO_3$ 26, $CaCl_2$ 2, and glucose 10, and was oxygenated with 95% O_2 / 5% CO_2 (pH = 7.3-7.4). 350 µm thick coronal slices containing the Nucleus Accumbens (NAc) core were

made with a vibratome (Leica VT 1200S) and incubated in oxygenated ACSF at room temperature for > 30 min. Slices were placed in an immersion recording chamber and superfused (2 ml/min) with oxygenated ACSF and visualized with an Olympus BX50WI microscope (Olympus Optical, Japan) or an Olympus BX61Wl confocal microscope (Olympus Optical, Japan).

Electrophysiology: The whole-cell patch clamp technique was used to make electrophysiological recordings of NAc core neurons. When filled with an internal solution containing (in mM): $KMeSO_4$ 135, KCl 10, HEPES 10, NaCl 5, ATP-Mg^{+2} 2.5, and GTP-Na^{+} 0.3 (pH = 7.3), patch electrodes exhibited a resistance of 3-10 MΩ. The membrane potential of neurons was held at -70 mV. Series and input resistances were monitored throughout the experiment using a -5 mV pulse. For some experiments, astrocytes were patched with 4-9 MΩ electrodes filled with an internal solution containing (in mM): $KMeSO_4$ 100, KCl 50, HEPES-K 10, and ATP-Na^{+2} 4 (pH=7.3). Astrocytes membrane potential was held at -80 mV. GDPßS (10 mM) and 0.5% biocytin were included in the astrocyte patch pipette. GDPßS was included to prevent G protein-mediated intracellular signaling in astrocytes. Astrocyte whole-cell recordings lasted at least 15-25 min to allow the dialysis of GDPßS throughout the gap-junction connected astrocyte network. Then, a relatively distant neuron (> 60 μm away from the recorded astrocyte) within the same field of view was patch-clamp recorded to monitor EPSCs (Navarrete and Araque, 2010). Signals were recorded with PC-ONE amplifiers (Dagan Instruments, MN, US) and fed to a Pentium-based PC through a DigiData 1440A interface board. Signals were filtered at 1 KHz and acquired at 10 KHz sampling rate. The pCLAMP 10.4 (Axon instruments) software was used for stimulus generation, data display, acquisition and storage.

Synaptic stimulation and drug application: Synaptic currents were evoked using bipolar theta capillaries filled with ACSF placed in the brain region of study (NAc core). Paired pulses (2 ms duration with 50 ms interval) were continuously delivered at 0.33 Hz using a stimulator S-910 through an isolation unit. Excitatory post-synaptic currents (EPSCs) were isolated using picrotoxin (50 μM) and CGP5462 (1 μM) to block $GABA_AR$ and $GABA_BR$, respectively. The measures analyzed were mean amplitude of EPSC response and paired pulse ratio (PPR=2^{nd} EPSC/1^{st} EPSC). For exogenous dopamine (500 μM), adenosine (250 μM) and CNO (1 mM) application, a borosilicate glass pipette containing the drug was placed over the NAc core and it was applied with a pressure pulse (0.5 bar, 5 s). For SKF 38393 application a borosilicate glass pipette containing SKF 38393 (500 μM) was placed over the NAc core and it was applied with a pressure

pulse (0.5 bar, 60 s). For optical stimulation of dopamine axons, an optic fiber connected to an LED (620 nm) was placed over the NAc core and a light train (5ms pulses for 5 s) of 0.1, 1, 10, 20, 30 or 50 Hz was applied. EPSC amplitudes were grouped in 15 s time bins, baseline mean EPSC amplitude was obtained by averaging mean values obtained within 2 min of baseline recordings and mean EPSC amplitudes were normalized to baseline. Stimulus (dopamine, CNO or optostimulation) effects were statistically tested comparing the normalized EPSCs recorded 15 s before and after the stimulus to assess changes in EPSC amplitude and PPR. For amphetamine experiments, EPSC amplitudes were grouped in 1 minute time bins and EPSC obtained 1 minute before and 20 minutes after amphetamine were compared to assess changes in EPSC amplitude. The effects of the pharmacological compounds on dopamine, CNO or optostimulation application were tested after having performed the stimulation in control conditions (dopamine, CNO or optostimulation without the pharmacological compound).

***In vitro* Ca^{2+} imaging:** Cytoplasmic Ca^{2+} levels in astrocytes in the NAc core were monitored using epifluorescence and confocal microscopy. Epifluorescence imaging utilized a CCD camera (Hammamatsu, Japan). Cells were illuminated during 100-200 ms with an LED at 490 nm (Prior Scientifics, MA, US) and images were acquired every 1-2 s. The LED and the CCD camera were controlled and synchronized by the MetaMorph software (Molecular devices). Confocal imaging utilized an Olympus BX61Wl confocal microscope (Olympus Optical, Japan) controlled by the Fluoview software or a Leica SP5 multi-photon microscope (Leica Microsystems, USA) controlled by the Leica LAS software. For control and pharmacology experiments Ca^{2+} was monitored using the genetically encoded Ca^{2+} indicator dye GCaMP3 under the glutamate aspartate transporter (GLAST) promoter (Figure S2A and S2B). For transgenic mice, that did not constitutively express GCaMP3, we used GCaMP6 under the GfaABC1D promoter to specifically target astrocytes (Figure S2C) or Fluo4. For experiments using fluo-4, slices were incubated with fluo-4-AM (2 μM and 0.01 % of pluronic) for 60 min at room temperature. Where noted, Ca^{2+} experiments were performed in the presence of TTX (1 μM) and a cocktail of neurotransmitter receptor antagonists containing: CNQX (20 μM), AP5 (50 μM), MPEP (50 μM), LY367385 (100 μM), picrotoxin (50 μM), CGP5462 (1 μM), atropine (50 μM), CPT (10 μM), and suramin (100 μM). TTX (1 μM) was always present in Ca^{2+} imaging experiments testing exogenous dopamine or amphetamine application, but not in experiments using optogenetic stimulation or assessing synaptic transmission.

ImageJ software (NIH) was used to quantify fluorescence level measurements in astrocytes. Ca^{2+} variations recorded at the soma and processes of the cells were estimated as changes of the fluorescence signal over baseline ($\Delta F/F_0$), and cells were considered to show a Ca^{2+} event when the $\Delta F/F_0$ increase was at least two times the standard deviation of the baseline and the astrocyte was considered to respond to the stimulus if the Ca^{2+} event occurred within 10 s after the stimulation. The astrocyte Ca^{2+} signal was quantified from the Ca^{2+} event probability, which was calculated from the number of Ca^{2+} elevations grouped in 10 s bins recorded from 2-50 astrocytes per field of view. The time of occurrence was considered at the onset of the Ca^{2+} event. For each astrocyte analyzed, values of 0 and 1 were assigned for bins showing either no response or a Ca^{2+} event, respectively, and the Ca^{2+} event probability was obtained by dividing the number of astrocytes showing an event at each time bin by the total number of monitored astrocytes. To examine the difference in Ca^{2+} event probability in distinct conditions, the basal Ca^{2+} event probability (10 seconds before a stimulus) was averaged and compared to the average Ca^{2+} event probability (10 seconds after a stimulus). The Ca^{2+} oscillation frequency was used for amphetamine experiments due to the mechanism of action of amphetamine and the evaluation of Ca^{2+} oscillations over a minute-timescale. In slice experiments using amphetamine (10 μM), the astrocyte Ca^{2+} signal was quantified from the Ca^{2+} oscillation frequency, which was obtained from the number of Ca^{2+} events occurring in 2-50 astrocytes per the field of view during 1 min periods. To establish magnitude correlations in Figure 3D and 3F, we examined the maximum values of the Ca^{2+} event probability and EPSC depression occurring within 15 s after the stimulation.

Stereotaxic Surgery: Adult mice were anesthetized with a ketamine (100 mg/kg)/ xylazine (10mg/kg) cocktail. Viral vectors (0.5μl-1μl) were injected bilaterally using a Hamilton syringe attached to a 29-gauge needle at a rate of 0.8-1.25 μl/min. The viral constructs AAV8-GFAP-hM3D(Gq)-mCherry (UNC vector core), AAV8-GFAP-mCherry (UMN vector core), AAV5-GfaABC1D-PI-LckGCaMP6.SV40 (Penn Vector Core), or AAV5-GfaABC1D-cytoGCaMP6f-SV40 (Penn Vector Core) were targeted to NAc core astrocytes (anterior-posterior[AP]: +1.50 mm; medial-lateral [ML]: +/- 0.75 mm; dorsal-ventral [DV]: -4.50 mm) of C57BL/6J. The AAV8-GFAP-mCherry-Cre viral vector (UNC vector core) was targeted to NAc core astrocytes of DrD1 flox/flox mice (homozygous and wild-type littermate mice). The AAV5-hSyn-FLEX-ChrimsonR-tdT (UNC vector core) was targeted to dopaminergic neurons in the VTA of DAT-IRES-Cre mice and wild-type litter-mate mice (anterior-posterior [AP]: -3 mm;

medial-lateral [ML]: +/- 0.5 mm; dorsal-ventral [DV]: - 4.3 mm). For some experiments, AAV5-GfaABC1D-PI-LckGCaMP6.SV40 (Penn Vector Core) or AAV5-GfaABC1D-cytoGCaMP6f-SV40 (Penn Vector Core) was also injected in the NAc core of DAT-IRES-Cre mice to monitor astrocyte Ca^{2+} signals. Mice were used ≥ 2 weeks after stereotaxic surgeries.

Fiber Photometry: We utilized fiber photometry to assess astrocyte Ca^{2+} activity and responsiveness to dopamine and amphetamine in freely behaving mice. In DAT-IRES-Cre mice, AAV5-hSyn-FLEX-ChrimsonR-tdT (0.5 μl; UNC vector core) was targeted to dopaminergic neurons in the VTA (anterior-posterior [AP]: -3 mm; medial-lateral [ML]: +/- 0.5 mm; dorsal-ventral [DV]: - 4.3 mm) and AAV5-GfaABC1D-cytoGCaMP6f-SV40 (1 μl; Penn Vector Core) or AAV5-GfaABC1D-PI-Lck-GFP-SV40 (1 μl; addgene) was targeted to NAc core astrocytes (anterior-posterior[AP]: +1.50 mm; medial-lateral [ML]: +/- 0.75 mm; dorsal-ventral [DV]: -4.50 mm) and the optic fiber (400μm, Doric Lenses: MFC_400/430-0.48_6mm_MF2.5_FLT) was placed 0.02 mm dorsal to NAc core viral infusion. The implant was attached to the skull with a dual-cure resin-ionomer (DenMat). Experiments were performed ≥ 3 weeks after surgery.

For data acquisition, the RZ5P processor (Tucker Davis Technologies) was utilized. A fluorescence mini-cube (Doric Lenses) was coupled to a 470 nm LED (Thorlabs M470F3; modulated at 211 Hz), a 405 nm LED (Thorlabs M405F1; modulated at 531 Hz) and a 595 nm LED (Thorlabs M595F2; for optogenetic stimulation of dopaminergic terminals expressing ChrimsonR). The fluorescence mini-cube was coupled to a patch cable and the opposite end was connected to the implanted optic fiber on the mice. GCaMP6f fluorescence from astrocytes was transmitted back through the cable to the mini-cube and focused onto the photoreceiver (Newport Model 2151, FC adapter). The sampling rate for the signals was 6.1 kHz. For each stimulation parameter (5 ms pulses for 5 s at 5, 10, 20, 30 or 50 Hz) mice were stimulated 3-5 times with a 2 minute inter-stimulation interval. For analysis, individual stimulations from control and pharmacological conditions (flupenthixol or amphetamine) were averaged and compared.

For data analysis, active (470 nm) and reference (405 nm) photometry signals were corrected for bleaching by fitting to an exponential function. The normalized signal was created via examining change in fluorescence ([470nm signal − fitted 405nm signal]/[fitted 405nm signal]). Custom MATLAB code was utilized to analyze the normalized data.

Brains from all mice used in fiber photometry experiments were analyzed to check adequate fiber location and proper and selective viral expression. Animals that did not meet the criteria for proper fiber location and virus expression were discarded.

Acute amphetamine locomotor-sensitivity: Male and female $IP_3R2^{-/-}$ mice (n = 18; n = 8 males and n = 10 females), $IP_3R2^{-/-}$ control wild-type background mice (Black Swiss; n = 16; n = 5 males and n = 11 females), GFAP-$D_1^{-/-}$ mice (n = 6; n = 3 males and n = 3 females;) and GFAP-D_1^{WT} (n = 6; n = 3 males and n = 3 females) were used for behavioral experiments. Mice were ≥ 5 weeks of age. Mice were handled by experimenter for at least two days before behavioral testing commenced. To habituate animals to i.p. injections and experimental conditions, mice were injected with saline for two consecutive days. On experimental day, mice were injected with amphetamine (2.5 mg/kg, i.p. for $IP_3R2^{-/-}$ mice and 5 mg/kg for GFAP-$D1^{-/-}$ mice experiments). On test days, mice were placed in locomotor chambers for 30 minutes to habituate to the environment, followed by drug administration (saline or amphetamine) and 60 minutes of locomotor tracking post-injection. Locomotor activity was tracked automatically using a camera tracking system and ANY-maze software (Stoelting Co.). A two-way repeated measures ANOVA was used to analyze the data.

Immunohistochemistry: The animals were anesthetized with Avertin (2,2,2 tribromoethanol, 240 mg/kg, i.p.) and intracardially perfused with ice cold phosphate buffered saline (PBS) and subsequently with 4% paraformaldehyde (PFA) in 0.1 M phosphate buffered saline (pH 7.4). The brain was removed and 40 μm coronal sections were made using a Leica VT1000S vibratome. Vibratome sections were incubated for one hour in blocking buffer (0.1% Triton X-100, 10% Donkey or Goat serum in PBS) at room temperature. The primary antibodies were diluted in the blocking solution and the sections were incubated overnight at 4°C. The following primary antibodies were used: Sheep anti-TH (Pel-Freez, 1:500), Mouse anti-NeuN (Millipore, 1:500), Rabbit anti-NeuN (Millipore; 1:500), Rabbit anti-GFAP (Sigma, 1:500), Mouse anti-NG2 (Millipore; 1:500), Rabbit anti-Iba1 (Dako; 1:500). The slices were washed three times for ten minutes each in 0.1M PBS. The secondary antibodies were diluted in the secondary antibody buffer (0.1% Triton X-100, 5% Donkey or Goat serum in PBS) and incubated for 2 hours at room temperature. The following secondary antibodies were used: 488 donkey anti-sheep (Invitrogen, 1:500), 405 goat anti–mouse (Invitrogen, 1:500) 488 goat anti-rabbit (Invitrogen, 1:1000). The sections were then washed 3 times with 1xPBS for 10 minutes

each and mounted using Vectashield Mounting media (Vector laboratories). Mounted slices were imaged using a Leica SP5 multi-photon microscope.

The cellular specificity of GCaMP3, GCaMP6, DREADD and Cre viral vectors was tested by immohistochemical analysis of randomly selected areas of the NAc. Out of the 511 cells expressing GCaMP3 from GLAST-GCaMP3 mice, 99% were astrocytes (identified by GFAP), 0.6% were neurons (identified by NeuN), 0% were oligodendrocytes (identified by NG2) and 0.4% were microglia (identified by Iba1) (Figure S2A and S2B). Out of the 192 cells expressing GCaMP6 from the AAV5-GfaABC1D-cytoGCaMP6f-SV40 viral vector, 99% were astrocytes (identified by GFAP), 0% were neurons (identified by NeuN), 0% were oligodendrocytes (identified by NG2) and 1% were microglia (identified by Iba1) (Figure S2C). Out of the 408 cells expressing mCherry from the AAV8-GFAP-hM3D(Gq)-mCherry viral vector, 99.01% were astrocytes (identified by GFAP), 0.25% were neurons (identified by NeuN), 0% were oligodendrocytes (identified by NG2) and 0.74% were microglia (identified by Iba1) (Figure S5A-C). Out of the 985 cells expressing mCherry from the AAV8-GFAP-mCherry-Cre viral vector, 87.6% were astrocytes (identified by GFAP), 11.9% were neurons (identified by NeuN), 0% were oligodendrocytes (identified by NG2) and 0.5% were microglia (identified by Iba1) (Figure S4A and S4B).

For biocytin labeling single astrocytes were recorded with patch pipettes and filled with internal solution containing 0.5% biocytin. Slices were fixed in 4% PFA in 0.1 PBS (pH 7.4) at 4°C. Slices were washed three times in 1xPBS (10 minutes each). To visualize biocytin slices were incubated with Alexa488-Streptavidin (RRID:AB 2315383; 1:500) for 48 hours at 4°C. Slices were then washed for 3 times with 1xPBS (10 minutes each) and mounted with Vectashield mounting media (Vector laboratories). All mounted slices were imaged using a Leica SP5 multi-photon microscope. The cellular specificity of biocytin labeling was assessed by immohistochemical analysis of randomly selected areas of the NAc. Out of 127 cells expressing biocytin, 5% were oligodendrocytes (identified by NG2).

Tissue preparation for electron microscopy: Three mice, obtained from the Animal House Facility (School of Medicine, University of Castilla-La Mancha), were used in this study for pre-embedding immunohistochemical analyses. The care and handling of animals prior to and during the experimental procedures were in accordance with Spanish (RD 1201/2005) and

European Union (86/609/EC) regulations, and the protocols were approved by the University's Animal Care and Use Committee.

Animals were anaesthetized by intraperitoneal injection of ketamine/xylazine 1:1 (0.1 mL/kg b.w.) and transcardially perfused with ice-cold fixative containing 4% paraformaldehyde, with 0.05% glutaraldehyde and 15% (v/v) saturated picric acid made up in 0.1 M phosphate buffer (PB, pH 7.4). After perfusion, brains were removed and immersed in the same fixative for 2 hours or overnight at 4°C. Tissue blocks were washed thoroughly in 0.1 M PB. Coronal 60 μm thick sections were cut on a Vibratome (Leica V1000).

Antibodies and chemicals for electron microscopy: The following primary antibodies were used: guinea pig anti-D1R polyclonal (GP-Af500; C-terminus 45 aa. of mouse D1R, NM010076; Frontier Institute co., Japan). The characteristics and specificity of the antibody targeting D1R has been described elsewhere (Narushima et al., 2006; Uchigashima et al., 2007). The secondary antibodies used were goat anti-guinea pig IgG coupled to 1.4 nm gold (1:100; Nanoprobes Inc., Stony Brook, NY, USA).

Immunohistochemistry for electron microscopy: Immunohistochemical reactions for electron microscopy were carried out using the pre-embedding immunogold method described previously (Lujan et al., 1996). Briefly, free-floating sections were incubated in 10% (v/v) NGS diluted in TBS. Sections were then incubated in anti-D1R antibodies [3-5 μg/mL diluted in TBS containing 1% (v/v) NGS], followed by incubation in goat anti-guinea pig IgG coupled to 1.4 nm gold (Nanoprobes Inc., Stony Brook, NY, USA), respectively. Sections were postfixed in 1% (v/v) glutaraldehyde and washed in double-distilled water, followed by silver enhancement of the gold particles with an HQ Silver kit (Nanoprobes Inc.). Sections were then treated with osmium tetraoxide (1% in 0.1 m phosphate buffer), block-stained with uranyl acetate, dehydrated in graded series of ethanol and flat-embedded on glass slides in Durcupan (Fluka) resin. Regions of interest were cut at 70-90 nm on an ultramicrotome (Reichert Ultracut E, Leica, Austria) and collected on single slot pioloform-coated copper grids. Staining was performed on drops of 1% aqueous uranyl acetate followed by Reynolds's lead citrate. Ultrastructural analyses were performed in a Jeol-1010 electron microscope.

Statistics: Data are expressed as mean ± standard error of the mean (SEM). For electrophysiology comparisons number of neurons was used as the sample size; for *in vitro* Ca^{2+} signal comparisons the number of slices was used as the sample size; for fiber photometry and

behavior comparisons the number of mice was used as the sample size. At least 3 mice per experimental group were used. Data normality was tested using a Kolmogorov-Smirnov test. Results were compared using a two-tailed Student's *t*-test or ANOVA ($\alpha = 0.05$). One way ANOVA with a Fisher LSD method post hoc was used for normal distributed data and Kruskal-Wallis One Way ANOVA with Dunn's method post hoc was used for non-normal distributed data. A full report of the statistics used in every case is detailed in Extended data Tables 1-3. Statistical differences were established with $p < 0.05$ (*), $p < 0.01$ (**) and $p < 0.001$ (***).

Drugs: 4-[3-[2-(Trifluoromethyl)-9*H*-thioxanthen-9-ylidene]propyl]-1-piperazineethanol dihydrochloride (flupenthixol dihydrochloride), [*S*-(*R**,*R**)]-[3-[[1-(3,4-Dichlorophenyl)ethyl]amino]-2-hydroxypropyl](cyclohexylmethyl) phosphinic acid (CGP 54626 hydrochloride), 8,8'-[Carbonyl*bis*[imino-3,1-phenylenecarbonylimino(4-methyl-3,1-phenylene)carbonylimino]]*bis*-1,3,5-naphthalenetrisulfonic acid hexasodium salt (suramin hexasodium salt), *N*-(Piperidin-1-yl)-5-(4-iodophenyl)-1-(2,4-dichlorophenyl)-4-methyl-1*H*-pyrazole-3-carboxamide (AM 251), D-(-)-2-Amino-5-phosphonopentanoic acid (D-AP5), 6-Cyano-7-nitroquinoxaline-2,3-dione disodium (CNQX disodium salt), (*S*)-(+)-α-Amino-4-carboxy-2-methylbenzeneacetic acid (LY367385), and 2-Methyl-6-(phenylethynyl)pyridine hydrochloride (MPEP hydrochloride), Octahydro-12-(hydroxymethyl)-2-imino-5,9:7,10a-dimethano-10a*H*-[1,3]dioxocino[6,5-*d*]pyrimidine-4,7,10,11,12-pentol (Tetrodotoxin: TTX) were purchased from Tocris Bioscience. Picrotoxin from Indofine Chemical Company (Hillsborough, NJ). Fluo-4-AM from Molecular Probes (Eugene, OR). All other drugs were purchased from Sigma.

FIGURE LEGENDS

Figure 1. Astrocytes respond to dopamine *in vivo*.

(A) Viral vectors used and image from DAT-cre mice showing expression of ChrimsonR in the VTA and expression of GCaMP6f and the optic fiber track (dotted line) in the NAc. NAc: nucleus accumbens, VTA: ventral tegmental area. (**B)** Scheme showing the fiber photometry system (*left*) and astrocyte responses to ChrimsonR activation (5 s, 30 Hz) in the NAc (*right*). (**C)** Mean astrocyte responses to distinct stimulation frequencies. (**D)** Mean fluorescence amplitude in response to ChrimsonR activation in the different experimental conditions (n = 19 stimuli from 5 animals for control, n = 14 stimuli from 2 animals for flupenthixol, n = 6 stimuli from 2 animals for GFP and n = 23 stimuli from 4 animals for Cre negative). Kruskal-Wallis One Way ANOVA. (**E)** Mean astrocyte responses to ChrimsonR activation before and after amphetamine administration. (**F)** Mean fluorescence amplitude, response rise time and width before and after amphetamine administration (n = 19 responses from 5 animals). Two-tailed student's unpaired t-test. **(G)** Electron microscopy images showing D_1 receptors in astrocytes (green arrows), spines (brown arrows) axon terminals (blue arrows). ast: astrocyte, s: spine, at: axon terminal. Data are expressed as mean ± s.e.m., *p<0.05, **p<0.01.

Figure 2. Astrocytes respond to dopamine through D_1 receptors.

(A) Pseudocolor images showing the fluorescence intensities of a GCaMP3-expressing astrocytes before and after DA application (*top*), representative Ca^{2+} traces of astrocytes (*bottom left*; arrow indicates DA application) and raster plot showing the Ca^{2+} events recorded from all ROIs including astrocyte somas and processes (*bottom right*). (**B)** Ca^{2+} event probability over time in somas and processes (*left*) and Ca^{2+} event probability before (basal) and after DA application in different experimental conditions (*right*); All experimental conditions were performed in TTX (1 μM). Cocktail of neurotransmitter receptor antagonists contained: CNQX 20 μM, AP5 50 μM, MPEP 50 μM, LY367385 100 μM, picrotoxin 50 μM, CGP5462 1 μM, atropine 50 μM, CPT 10 μM, and suramin 100 μM). One way ANOVA and two-tailed student's paired t-test. **(C** and **D)** Same as **A** and **B** but using optostimulation of dopaminergic axons instead of DA application. Experiments were performed in CNQX 20 μM, AP5 50 μM, MPEP 50 μM, LY367385 100 μM, picrotoxin 50 μM, CGP5462 1 μM, atropine 50 μM, CPT 10 μM, and suramin 100 μM. One way ANOVA and two-tailed student's paired t-test. Blue and red shadows indicate DA application and optical stimulation, respectively. Data are expressed as mean ± s.e.m., *p<0.05, **p<0.01, ***p<0.001.

Figure 3. Dopamine stimulates astrocyte Ca^{2+} increases and neuronal excitatory transmission depression.

(A) Scheme of the experimental approach (*left*) and representative EPSC traces before (basal) and after DA application (*right*). **(B)** like **A** but for optical stimulation. **(C)** Ca^{2+} event probability and relative EPSC amplitude over time. **(D)** Relationship between Ca^{2+} event probability and change in EPSC amplitude after DA application. **(E** and **F)** The same as **C** and **D** but for optical stimulation. Blue and red shadows indicate DA application and optical stimulation, respectively. Data are expressed as mean ± s.e.m.

Figure 4. Astrocyte Ca^{2+} is necessary for DA-evoked synaptic depression.

(A) Scheme of the experimental approach (*top*) and fluorescence image of an astrocyte network loaded with biocytin through a patched astrocyte (*bottom*). **(B)** Ca^{2+} event probability and relative EPSC amplitude before (basal) and after DA application. Two-tailed student's paired t-test. **(C)** Viral vector injected into the NAc of D1-flox mice and fluorescence image showing mCherry-Cre expression in the NAc (*top*), and immunohistochemistry images showing co-localization between mCherry-cre and GFAP (*bottom*). **(D)** Ca^{2+} event probability over time (*left*) and Ca^{2+} event probability before (basal) and after DA or ATP application (*right*). Blue shadow indicates DA application. Two-tailed student's paired t-test. **(E)** Relative EPSC amplitude before (basal) and after DA application. Two-tailed student's paired t-test. Data are expressed as mean ± s.e.m., *$p<0.05$, ***$p<0.001$.

Figure 5. Astrocytes mediate DA-evoked synaptic depression via adenosine signaling.

(A) Ca^{2+} event probability before (basal) and after DA application or optogenetic stimulation. Two-tailed student's paired t-test. **(B)** Relative EPSC amplitude before (basal) and after DA application or optogenetic stimulation. Two-tailed student's paired t-test. **(C)** Scheme of experimental approach. **(D)** Relative EPSC amplitude over time. Blue and orange shadows indicate DA application and adenosine application, respectively. **(E)** Relative EPSC amplitude before (basal) and after DA application or adenosine application. Two-tailed student's paired t-test. **(F)** Schematic summary depicting the signaling pathways involved in DA-evoked synaptic depression. Data are expressed as mean ± s.e.m., **$p<0.01$, ***$p<0.001$.

Figure 6. Astrocyte Ca^{2+} is sufficient for excitatory synaptic depression.

(A) Viral vector injected into the NAc and fluorescence image showing DREADD-mCherry expression in the NAc (*top*). Scheme of the experimental approach (*bottom*). **(B)** Pseudocolor

images showing the fluorescence intensities of a GCaMP6f-expressing astrocytes before and after CNO application (*top*) and Ca^{2+} event probability before (basal) and after CNO application (*bottom*). Two-tailed student's paired t-test. **(C)** Representative EPSC traces before (basal) and after CNO application (*top*) and relative EPSC amplitude before (basal) and after CNO application (*bottom*). Two-tailed student's paired t-test. Data are expressed as mean ± s.e.m., *p<0.05, **p<0.01.

Figure 7. Astrocytes are involved in amphetamine synaptic effects.

(A) Representative Ca^{2+} traces of astrocytes in control (basal) and the presence of amphetamine. **(B)** Raster plots showing the Ca^{2+} events recorded from all ROIs including astrocyte somas and processes in control (basal) and the presence of amphetamine. **(C)** Ca^{2+} oscillation frequency over time. **(D)** Ca^{2+} oscillation frequency in control (basal) and in the presence of amphetamine. Two-tailed student's paired t-test. **(E)** Representative EPSC traces before (basal) and after amphetamine application. **(F)** Relative EPSC amplitude over time. **(G)** Relative EPSC amplitude before (basal) and in the presence of amphetamine. Two-tailed student's paired t-test. **(H)** Representative traces of locomotor activity of mice injected with saline or amphetamine. **(I)** Distance traveled of different mice injected with saline or amphetamine (for $IP_3R2^{-/-}$ mice: n = 18; n = 8 males and n = 10 females; for $IP_3R2^{-/-}$ control wild-type mice: n = 16; n = 5 males and n = 11 females; for GFAP-$D_1^{-/-}$ mice: n = 6; n = 3 males and n = 3 females; for GFAP-D_1^{WT} mice: n = 6; n = 3 males and n = 3 females). Two-tailed student's unpaired t-test. Green shadow indicates amphetamine application. Data are expressed as mean ± s.e.m., *p<0.05, **p<0.01, ***p<0.001.

REFERENCES

Araque, A., Carmignoto, G., and Haydon, P.G. (2001). Dynamic signaling between astrocytes and neurons. Annual review of physiology *63*, 795-813.

Araque, A., Carmignoto, G., Haydon, P.G., Oliet, S.H., Robitaille, R., and Volterra, A. (2014). Gliotransmitters travel in time and space. Neuron *81*, 728-739.

Araque, A., Parpura, V., Sanzgiri, R.P., and Haydon, P.G. (1999). Tripartite synapses: glia, the unacknowledged partner. Trends in neurosciences *22*, 208-215.

760 Bamford, N.S., Zhang, H., Joyce, J.A., Scarlis, C.A., Hanan, W., Wu, N.P., Andre, V.M., Cohen,
761 R., Cepeda, C., Levine, M.S., *et al.* (2008). Repeated exposure to methamphetamine causes long-
762 lasting presynaptic corticostriatal depression that is renormalized with drug readministration.
763 Neuron *58*, 89-103.
764 Beaulieu, J.M., and Gainetdinov, R.R. (2011). The physiology, signaling, and pharmacology of
765 dopamine receptors. Pharmacological reviews *63*, 182-217.
766 Bezzi, P., Gundersen, V., Galbete, J.L., Seifert, G., Steinhauser, C., Pilati, E., and Volterra, A.
767 (2004). Astrocytes contain a vesicular compartment that is competent for regulated exocytosis of
768 glutamate. Nature neuroscience *7*, 613-620.
769 Brito, V., Beyer, C., and Küppers, E. (2004). BDNF-dependent stimulation of dopamine D5
770 receptor expression in developing striatal astrocytes involves PI3-kinase signaling. Glia *46*, 284-
771 295.
772 Calipari, E.S., and Ferris, M.J. (2013). Amphetamine mechanisms and actions at the dopamine
773 terminal revisited. The Journal of neuroscience : the official journal of the Society for
774 Neuroscience *33*, 8923-8925.
775 Covelo, A., and Araque, A. (2016). Lateral regulation of synaptic transmission by astrocytes.
776 Neuroscience *323*, 62-66.
777 Covelo, A., and Araque, A. (2018). Neuronal activity determines distinct gliotransmitter release
778 from a single astrocyte. eLife *7*.
779 Cui, Q., Pitt, J.E., Pamukcu, A., Poulin, J.F., Mabrouk, O.S., Fiske, M.P., Fan, I.B., Augustine,
780 E.C., Young, K.A., Kennedy, R.T., *et al.* (2016). Blunted mGluR Activation Disinhibits
781 Striatopallidal Transmission in Parkinsonian Mice. Cell reports *17*, 2431-2444.

D'Ascenzo, M., Fellin, T., Terunuma, M., Revilla-Sanchez, R., Meaney, D.F., Auberson, Y.P., Moss, S.J., and Haydon, P.G. (2007). mGluR5 stimulates gliotransmission in the nucleus accumbens. Proceedings of the National Academy of Sciences of the United States of America *104*, 1995-2000.

Di Castro, M.A., Chuquet, J., Liaudet, N., Bhaukaurally, K., Santello, M., Bouvier, D., Tiret, P., and Volterra, A. (2011). Local Ca2+ detection and modulation of synaptic release by astrocytes. Nature neuroscience *14*, 1276-1284.

Gomez-Gonzalo, M., Martin-Fernandez, M., Martinez-Murillo, R., Mederos, S., Hernandez-Vivanco, A., Jamison, S., Fernandez, A.P., Serrano, J., Calero, P., Futch, H.S., *et al.* (2017). Neuron-astrocyte signaling is preserved in the aging brain. Glia *65*, 569-580.

Gomez-Gonzalo, M., Navarrete, M., Perea, G., Covelo, A., Martin-Fernandez, M., Shigemoto, R., Lujan, R., and Araque, A. (2015). Endocannabinoids Induce Lateral Long-Term Potentiation of Transmitter Release by Stimulation of Gliotransmission. Cerebral cortex *25*, 3699-3712.

Halassa, M.M., and Haydon, P.G. (2010). Integrated brain circuits: astrocytic networks modulate neuronal activity and behavior. Annual review of physiology *72*, 335-355.

Harvey, J., and Lacey, M.G. (1996). Endogenous and exogenous dopamine depress EPSCs in rat nucleus accumbens in vitro via D1 receptors activation. The Journal of physiology *492 (Pt 1)*, 143-154.

Harvey, J., and Lacey, M.G. (1997). A postsynaptic interaction between dopamine D1 and NMDA receptors promotes presynaptic inhibition in the rat nucleus accumbens via adenosine release. The Journal of neuroscience : the official journal of the Society for Neuroscience *17*, 5271-5280.

804 Haydon, P.G., and Carmignoto, G. (2006). Astrocyte control of synaptic transmission and
805 neurovascular coupling. Physiological reviews *86*, 1009-1031.
806 Henneberger, C., Papouin, T., Oliet, S.H., and Rusakov, D.A. (2010). Long-term potentiation
807 depends on release of D-serine from astrocytes. Nature *463*, 232-236.
808 Jennings, A., Tyurikova, O., Bard, L., Zheng, K., Semyanov, A., Henneberger, C., and Rusakov,
809 D.A. (2017). Dopamine elevates and lowers astroglial Ca2+ through distinct pathways depending
810 on local synaptic circuitry. Glia *65*, 447-459.
811 Jin, L.Q., Goswami, S., Cai, G., Zhen, X., and Friedman, E. (2003). SKF83959 selectively
812 regulates phosphatidylinositol-linked D1 dopamine receptors in rat brain. Journal of
813 neurochemistry *85*, 378-386.
814 Kalivas, P.W., and Volkow, N.D. (2005). The neural basis of addiction: a pathology of
815 motivation and choice. The American journal of psychiatry *162*, 1403-1413.
816 Klapoetke, N.C., Murata, Y., Kim, S.S., Pulver, S.R., Birdsey-Benson, A., Cho, Y.K., Morimoto,
817 T.K., Chuong, A.S., Carpenter, E.J., Tian, Z., *et al.* (2014). Independent optical excitation of
818 distinct neural populations. Nature methods *11*, 338-346.
819 Kombian, S.B., Ananthalakshmi, K.V., Parvathy, S.S., and Matowe, W.C. (2003). Substance P
820 depresses excitatory synaptic transmission in the nucleus accumbens through dopaminergic and
821 purinergic mechanisms. Journal of neurophysiology *89*, 728-737.
822 Lerner, T.N., Shilyansky, C., Davidson, T.J., Evans, K.E., Beier, K.T., Zalocusky, K.A., Crow,
823 A.K., Malenka, R.C., Luo, L., Tomer, R., *et al.* (2015). Intact-Brain Analyses Reveal Distinct
824 Information Carried by SNc Dopamine Subcircuits. Cell *162*, 635-647.

825 Lezcano, N., and Bergson, C. (2002). D1/D5 Dopamine Receptors Stimulate Intracellular
826 Calcium Release in Primary Cultures of Neocortical and Hippocampal Neurons. Journal of
827 Neurophysiology *87*, 2167-2175.
828 Li, X., Zima, A.V., Sheikh, F., Blatter, L.A., and Chen, J. (2005). Endothelin-1-induced
829 arrhythmogenic Ca2+ signaling is abolished in atrial myocytes of inositol-1,4,5-
830 trisphosphate(IP3)-receptor type 2-deficient mice. Circulation research *96*, 1274-1281.
831 Lujan, R., Nusser, Z., Roberts, J.D., Shigemoto, R., and Somogyi, P. (1996). Perisynaptic
832 location of metabotropic glutamate receptors mGluR1 and mGluR5 on dendrites and dendritic
833 spines in the rat hippocampus. The European journal of neuroscience *8*, 1488-1500.
834 Luscher, C. (2016). The Emergence of a Circuit Model for Addiction. Annual review of
835 neuroscience *39*, 257-276.
836 Luscher, C., and Malenka, R.C. (2011). Drug-evoked synaptic plasticity in addiction: from
837 molecular changes to circuit remodeling. Neuron *69*, 650-663.
838 Lüscher, C., and Malenka, Robert C. (2011). Drug-Evoked Synaptic Plasticity in Addiction:
839 From Molecular Changes to Circuit Remodeling. Neuron *69*, 650-663.
840 Martin-Fernandez, M., Jamison, S., Robin, L.M., Zhao, Z., Martin, E.D., Aguilar, J.,
841 Benneyworth, M.A., Marsicano, G., and Araque, A. (2017). Synapse-specific astrocyte gating of
842 amygdala-related behavior. Nature neuroscience *20*, 1540-1548.
843 Martin, E.D., Fernandez, M., Perea, G., Pascual, O., Haydon, P.G., Araque, A., and Cena, V.
844 (2007). Adenosine released by astrocytes contributes to hypoxia-induced modulation of synaptic
845 transmission. Glia *55*, 36-45.
846 Martin, R., Bajo-Graneras, R., Moratalla, R., Perea, G., and Araque, A. (2015). Circuit-specific
847 signaling in astrocyte-neuron networks in basal ganglia pathways. Science *349*, 730-734.

Medvedev, I.O., Ramsey, A.J., Masoud, S.T., Bermejo, M.K., Urs, N., Sotnikova, T.D., Beaulieu, J.-M., Gainetdinov, R.R., and Salahpour, A. (2013). D₁ Dopamine Receptor Coupling to PLCβ Regulates Forward Locomotion in Mice. The Journal of Neuroscience *33*, 18125-18133.

Min, R., and Nevian, T. (2012). Astrocyte signaling controls spike timing-dependent depression at neocortical synapses. Nature neuroscience *15*, 746-753.

Min, R., Santello, M., and Nevian, T. (2012). The computational power of astrocyte mediated synaptic plasticity. Frontiers in computational neuroscience *6*, 93.

Miyazaki, I., Asanuma, M., Diaz-Corrales, F.J., Miyoshi, K., and Ogawa, N. (2004). Direct evidence for expression of dopamine receptors in astrocytes from basal ganglia. Brain research *1029*, 120-123.

Mori, T., Tanaka, K., Buffo, A., Wurst, W., Kuhn, R., and Gotz, M. (2006). Inducible gene deletion in astroglia and radial glia--a valuable tool for functional and lineage analysis. Glia *54*, 21-34.

Narushima, M., Uchigashima, M., Hashimoto, K., Watanabe, M., and Kano, M. (2006). Depolarization-induced suppression of inhibition mediated by endocannabinoids at synapses from fast-spiking interneurons to medium spiny neurons in the striatum. The European journal of neuroscience *24*, 2246-2252.

Navarrete, M., and Araque, A. (2010). Endocannabinoids potentiate synaptic transmission through stimulation of astrocytes. Neuron *68*, 113-126.

Navarrete, M., Perea, G., Fernandez de Sevilla, D., Gomez-Gonzalo, M., Nunez, A., Martin, E.D., and Araque, A. (2012). Astrocytes mediate in vivo cholinergic-induced synaptic plasticity. PLoS biology *10*, e1001259.

871 Nicola, S.M., Kombian, S.B., and Malenka, R.C. (1996). Psychostimulants depress excitatory
872 synaptic transmission in the nucleus accumbens via presynaptic D1-like dopamine receptors. The
873 Journal of neuroscience : the official journal of the Society for Neuroscience *16*, 1591-1604.
874 Nicola, S.M., and Malenka, R.C. (1997). Dopamine depresses excitatory and inhibitory synaptic
875 transmission by distinct mechanisms in the nucleus accumbens. The Journal of neuroscience : the
876 official journal of the Society for Neuroscience *17*, 5697-5710.
877 Nicola, S.M., Surmeier, D.J., and Malenka, R.C. (2000). Dopaminergic Modulation of Neuronal
878 Excitability in the Striatum and Nucleus Accumbens. Annual Review of Neuroscience *23*, 185-
879 215.
880 Panatier, A., Vallee, J., Haber, M., Murai, K.K., Lacaille, J.C., and Robitaille, R. (2011).
881 Astrocytes are endogenous regulators of basal transmission at central synapses. Cell *146*, 785-
882 798.
883 Parri, H.R., Gould, T.M., and Crunelli, V. (2001). Spontaneous astrocytic Ca2+ oscillations in
884 situ drive NMDAR-mediated neuronal excitation. Nature neuroscience *4*, 803-812.
885 Pascual, O., Casper, K.B., Kubera, C., Zhang, J., Revilla-Sanchez, R., Sul, J.Y., Takano, H.,
886 Moss, S.J., McCarthy, K., and Haydon, P.G. (2005). Astrocytic purinergic signaling coordinates
887 synaptic networks. Science *310*, 113-116.
888 Paukert, M., Agarwal, A., Cha, J., Doze, V.A., Kang, J.U., and Bergles, D.E. (2014).
889 Norepinephrine controls astroglial responsiveness to local circuit activity. Neuron *82*, 1263-
890 1270.
891 Perea, G., and Araque, A. (2007). Astrocytes potentiate transmitter release at single hippocampal
892 synapses. Science *317*, 1083-1086.

Perea, G., Gomez, R., Mederos, S., Covelo, A., Ballesteros, J.J., Schlosser, L., Hernandez-Vivanco, A., Martin-Fernandez, M., Quintana, R., Rayan, A., *et al.* (2016). Activity-dependent switch of GABAergic inhibition into glutamatergic excitation in astrocyte-neuron networks. eLife *5*.

Perea, G., Navarrete, M., and Araque, A. (2009). Tripartite synapses: astrocytes process and control synaptic information. Trends in neurosciences *32*, 421-431.

Petravicz, J., Fiacco, T.A., and McCarthy, K.D. (2008). Loss of IP3 receptor-dependent Ca2+ increases in hippocampal astrocytes does not affect baseline CA1 pyramidal neuron synaptic activity. The Journal of neuroscience : the official journal of the Society for Neuroscience *28*, 4967-4973.

Saunders, B.T., Richard, J.M., Margolis, E.B., and Janak, P.H. (2018). Dopamine neurons create Pavlovian conditioned stimuli with circuit-defined motivational properties. Nature neuroscience *21*, 1072-1083.

Scofield, M.D., Boger, H.A., Smith, R.J., Li, H., Haydon, P.G., and Kalivas, P.W. (2015). Gq-DREADD Selectively Initiates Glial Glutamate Release and Inhibits Cue-induced Cocaine Seeking. Biological psychiatry *78*, 441-451.

Serrano, A., Haddjeri, N., Lacaille, J.C., and Robitaille, R. (2006). GABAergic network activation of glial cells underlies hippocampal heterosynaptic depression. The Journal of neuroscience : the official journal of the Society for Neuroscience *26*, 5370-5382.

Surmeier, D.J., Bargas, J., Hemmings, H.C., Jr., Nairn, A.C., and Greengard, P. (1995). Modulation of calcium currents by a D1 dopaminergic protein kinase/phosphatase cascade in rat neostriatal neurons. Neuron *14*, 385-397.

915 Tang, T.S., and Bezprozvanny, I. (2004). Dopamine receptor-mediated Ca(2+) signaling in
916 striatal medium spiny neurons. The Journal of biological chemistry *279*, 42082-42094.
917 Tritsch, N.X., and Sabatini, B.L. (2012). Dopaminergic modulation of synaptic transmission in
918 cortex and striatum. Neuron *76*, 33-50.
919 Uchigashima, M., Narushima, M., Fukaya, M., Katona, I., Kano, M., and Watanabe, M. (2007).
920 Subcellular arrangement of molecules for 2-arachidonoyl-glycerol-mediated retrograde signaling
921 and its physiological contribution to synaptic modulation in the striatum. The Journal of
922 neuroscience : the official journal of the Society for Neuroscience *27*, 3663-3676.
923 Volterra, A., Liaudet, N., and Savtchouk, I. (2014). Astrocyte Ca(2)(+) signalling: an unexpected
924 complexity. Nature reviews Neuroscience *15*, 327-335.
925 Volterra, A., and Meldolesi, J. (2005). Astrocytes, from brain glue to communication elements:
926 the revolution continues. Nature reviews Neuroscience *6*, 626-640.
927 Wang, W., Dever, D., Lowe, J., Storey, G.P., Bhansali, A., Eck, E.K., Nitulescu, I., Weimer, J.,
928 and Bamford, N.S. (2012). Regulation of prefrontal excitatory neurotransmission by dopamine in
929 the nucleus accumbens core. The Journal of physiology *590*, 3743-3769.
930 Zhang, J.M., Wang, H.K., Ye, C.Q., Ge, W., Chen, Y., Jiang, Z.L., Wu, C.P., Poo, M.M., and
931 Duan, S. (2003). ATP released by astrocytes mediates glutamatergic activity-dependent
932 heterosynaptic suppression. Neuron *40*, 971-982.
933 Zhang, X., Zhou, Z., Wang, D., Li, A., Yin, Y., Gu, X., Ding, F., Zhen, X., and Zhou, J. (2009).
934 Activation of Phosphatidylinositol-Linked D₁-Like Receptor Modulates FGF-2
935 Expression in Astrocytes via IP3-Dependent Ca²⁺ Signaling. The Journal of
936 Neuroscience *29*, 7766-7775.

937

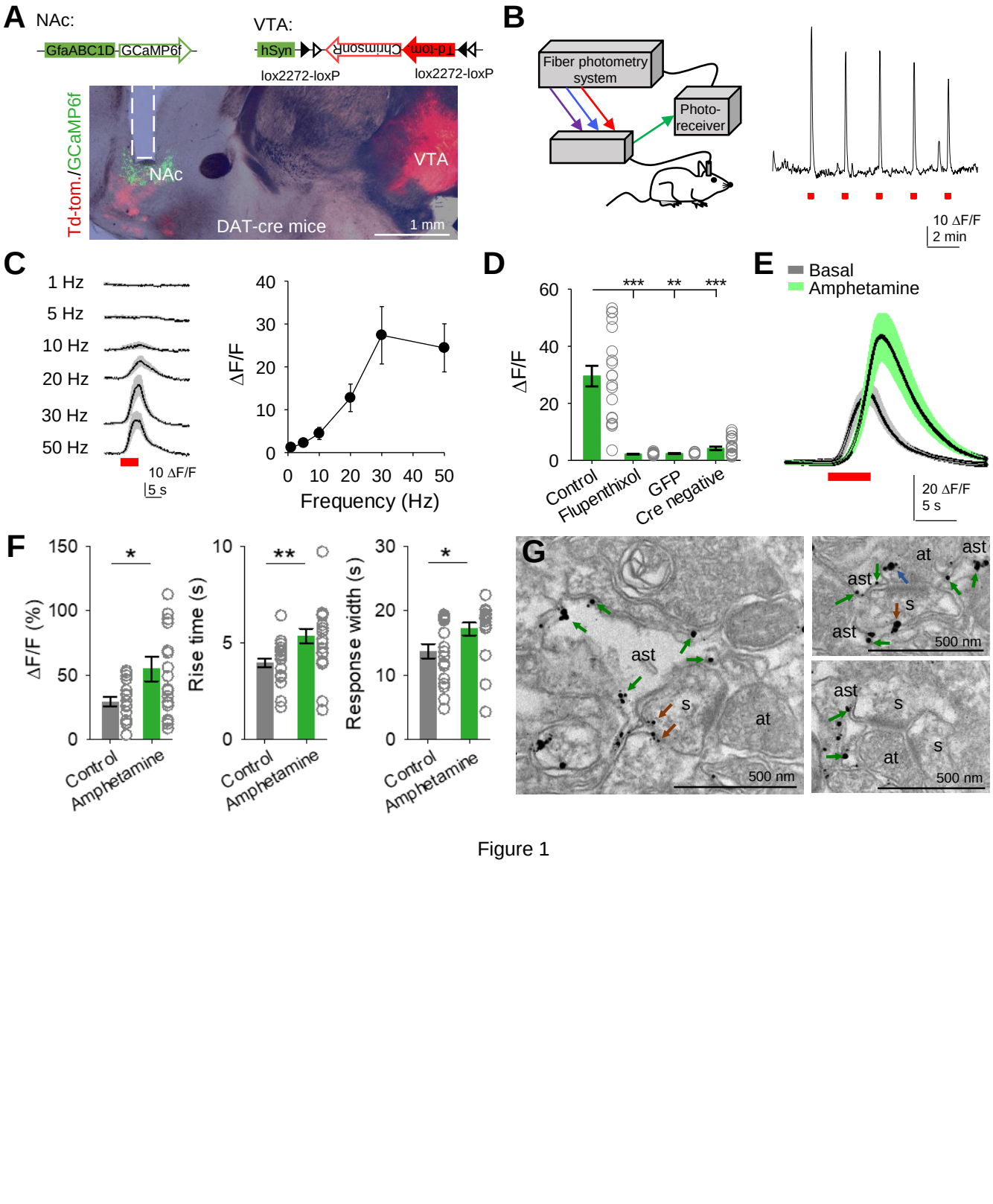
A
NAc:
GfaABC1D
GCaMP6f
VTA:
hSyn
Chrimsonr
Td-tom
lox2272-loxP
lox2272-loxP
Td-tom./GCaMP6f
NAc
VTA
DAT-cre mice
1 mm
B
Fiber photometry system
Photo-receiver
10 ΔF/F
2 min
C
1 Hz
5 Hz
10 Hz
20 Hz
30 Hz
50 Hz
10 ΔF/F
5 s
ΔF/F
Frequency (Hz)
D
ΔF/F
***
**
***
Control
Flupenthixol
GFP
Cre negative
E
Basal
Amphetamine
20 ΔF/F
5 s
F
ΔF/F (%)
Rise time (s)
Response width (s)
*
**
*
Control
Amphetamine
G
ast
s
at
500 nm

Figure 1

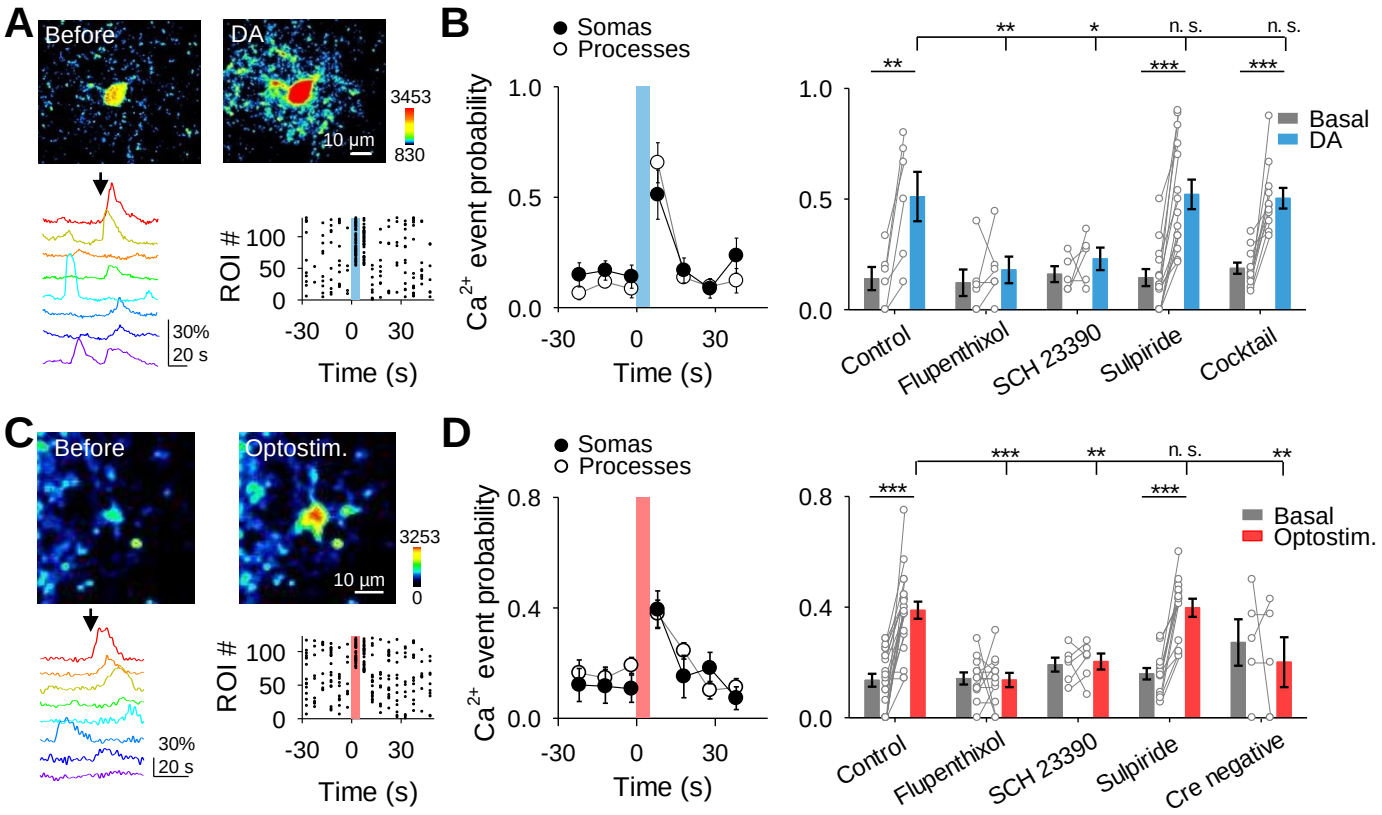
A
Before
DA
3453
830
10 µm
30%
20 s
ROI #
100
50
0
-30
0
30
Time (s)
B
Somas
Processes
Ca2+ event probability
1.0
0.5
0.0
-30
0
30
Time (s)
**
*
n. s.
n. s.
**
***
***
Basal
DA
Control
Flupenthixol
SCH 23390
Sulpiride
Cocktail
C
Before
Optostim.
3253
0
10 µm
30%
20 s
ROI #
100
50
0
-30
0
30
Time (s)
D
Somas
Processes
Ca2+ event probability
0.8
0.4
0.0
-30
0
30
Time (s)
***
**
n. s.
**
***
Basal
Optostim.
Control
Flupenthixol
SCH 23390
Sulpiride
Cre negative

Figure 2

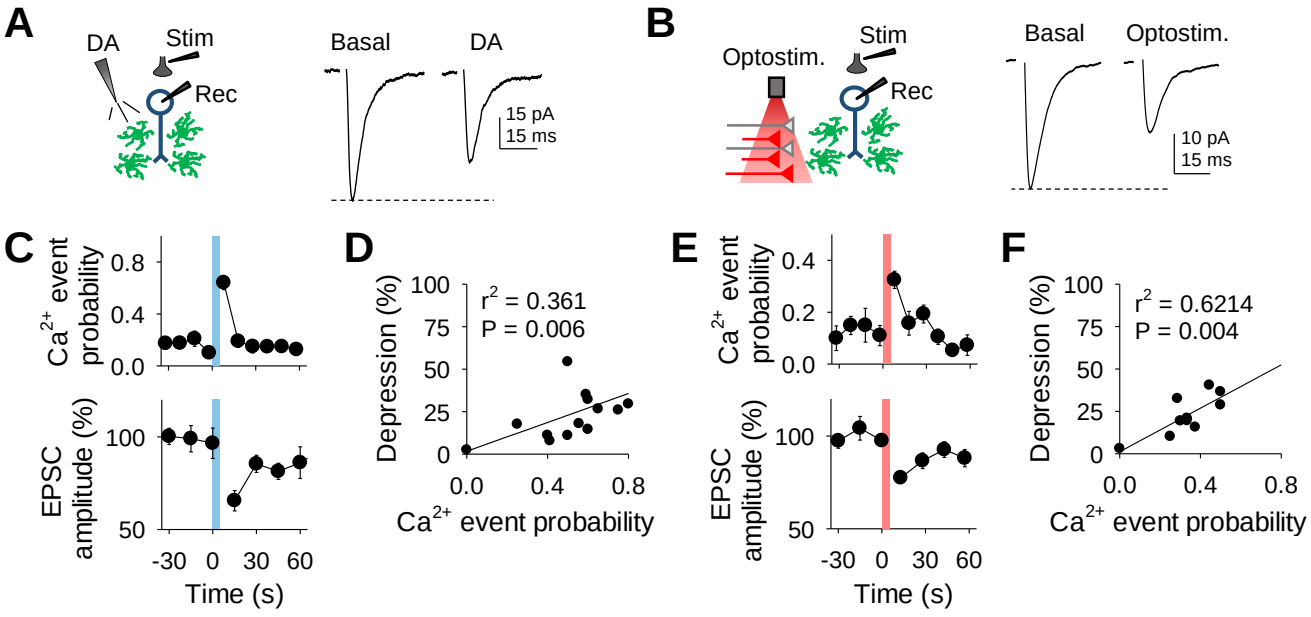
A
DA
Stim
Rec
Basal
DA
15 pA
15 ms
B
Optostim.
Stim
Rec
Basal
Optostim.
10 pA
15 ms
C
Ca2+ event probability
0.8
0.4
0.0
EPSC amplitude (%)
100
50
-30
0
30
60
Time (s)
D
Depression (%)
100
75
50
25
0
r2 = 0.361
P = 0.006
0.0
0.4
0.8
Ca2+ event probability
E
Ca2+ event probability
0.4
0.2
0.0
EPSC amplitude (%)
100
50
-30
0
30
60
Time (s)
F
Depression (%)
100
75
50
25
0
r2 = 0.6214
P = 0.004
0.0
0.4
0.8
Ca2+ event probability

Figure 3

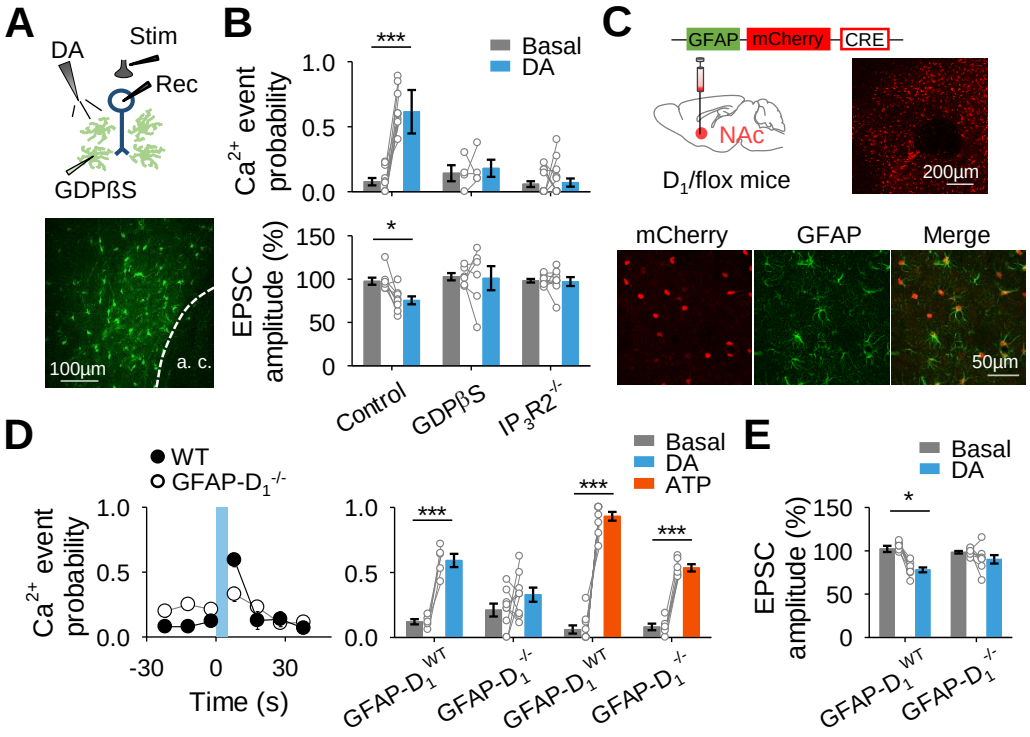
A
DA
Stim
Rec
GDPßS
100µm
a. c.
B
***
Basal
DA
Ca2+ event probability
1.0
0.5
0.0
*
EPSC amplitude (%)
150
100
50
0
Control
GDPßS
IP3R2-/-
C
GFAP
mCherry
CRE
NAc
D1/flox mice
200µm
mCherry
GFAP
Merge
50µm
D
WT
GFAP-D1-/-
Ca2+ event probability
-30
0
30
Time (s)
Basal
DA
ATP
GFAP-D1WT
GFAP-D1-/-
E
Basal
DA
EPSC amplitude (%)

Figure 4

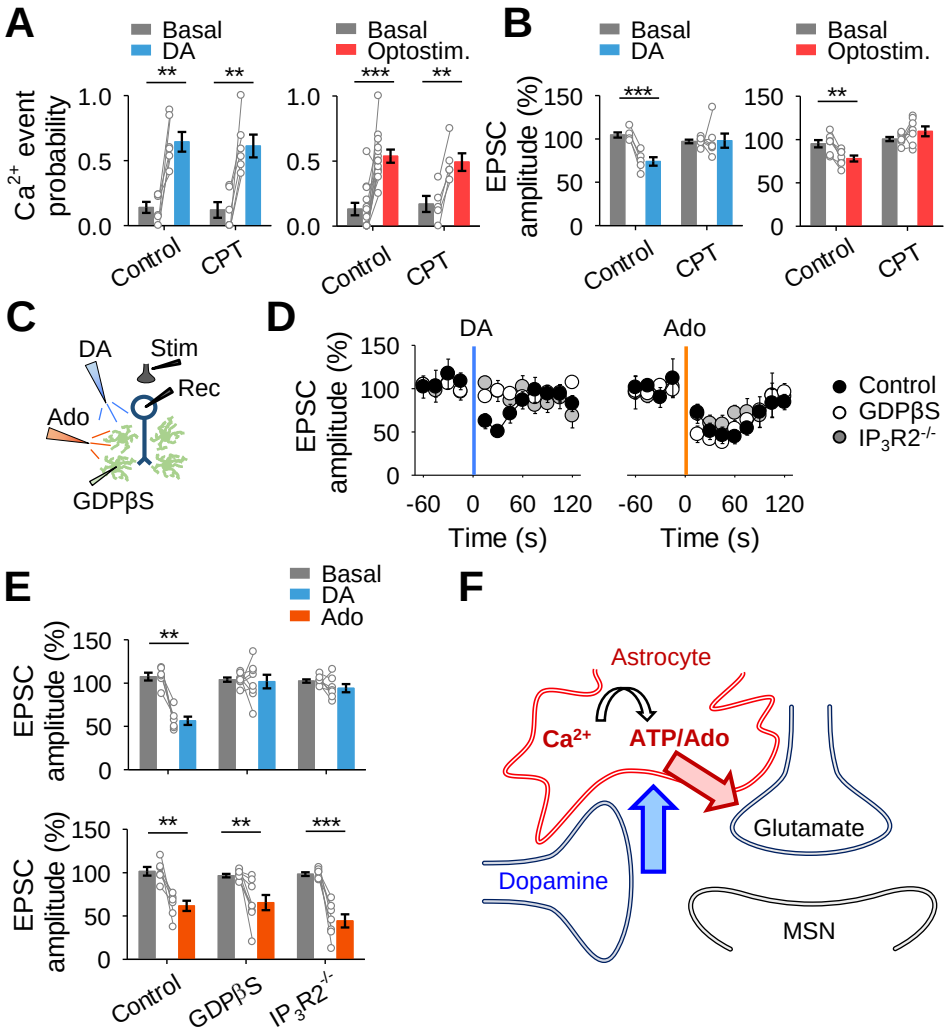
A
Basal
DA
Optostim.
Ca2+ event probability
1.0
0.5
0.0
**
***
Control
CPT
B
EPSC amplitude (%)
150
100
50
0
C
DA
Stim
Rec
Ado
GDPβS
D
Time (s)
-60
0
60
120
Control
GDPβS
IP3R2-/-
E
F
Astrocyte
Ca2+
ATP/Ado
Glutamate
Dopamine
MSN

Figure 5

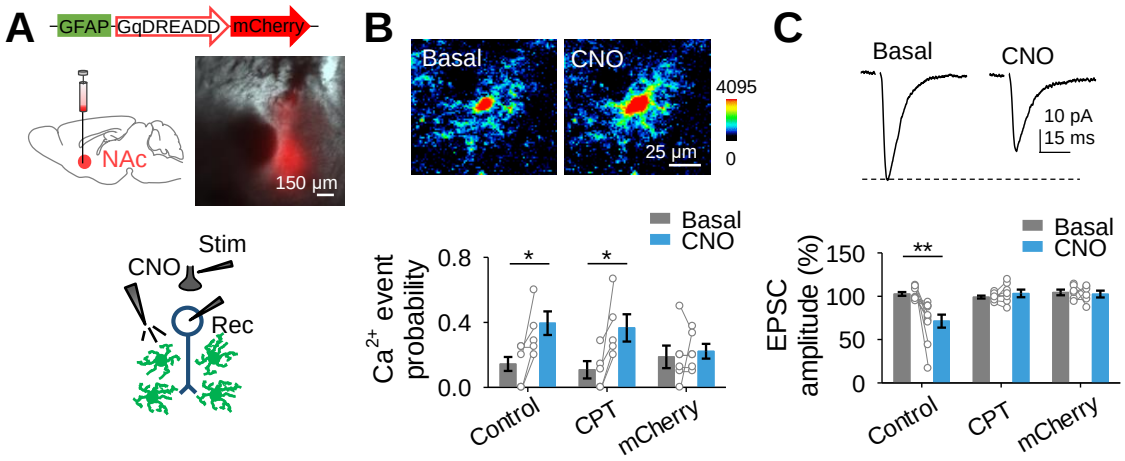
A
GFAP
GqDREADD
mCherry
NAc
150 μm
Stim
CNO
Rec
B
Basal
CNO
4095
0
25 μm
Basal
CNO
Ca2+ event probability
0.8
0.4
0.0
*
*
Control
CPT
mCherry
C
Basal
CNO
10 pA
15 ms
Basal
CNO
EPSC amplitude (%)
150
100
50
0
**
Control
CPT
mCherry

Figure 6

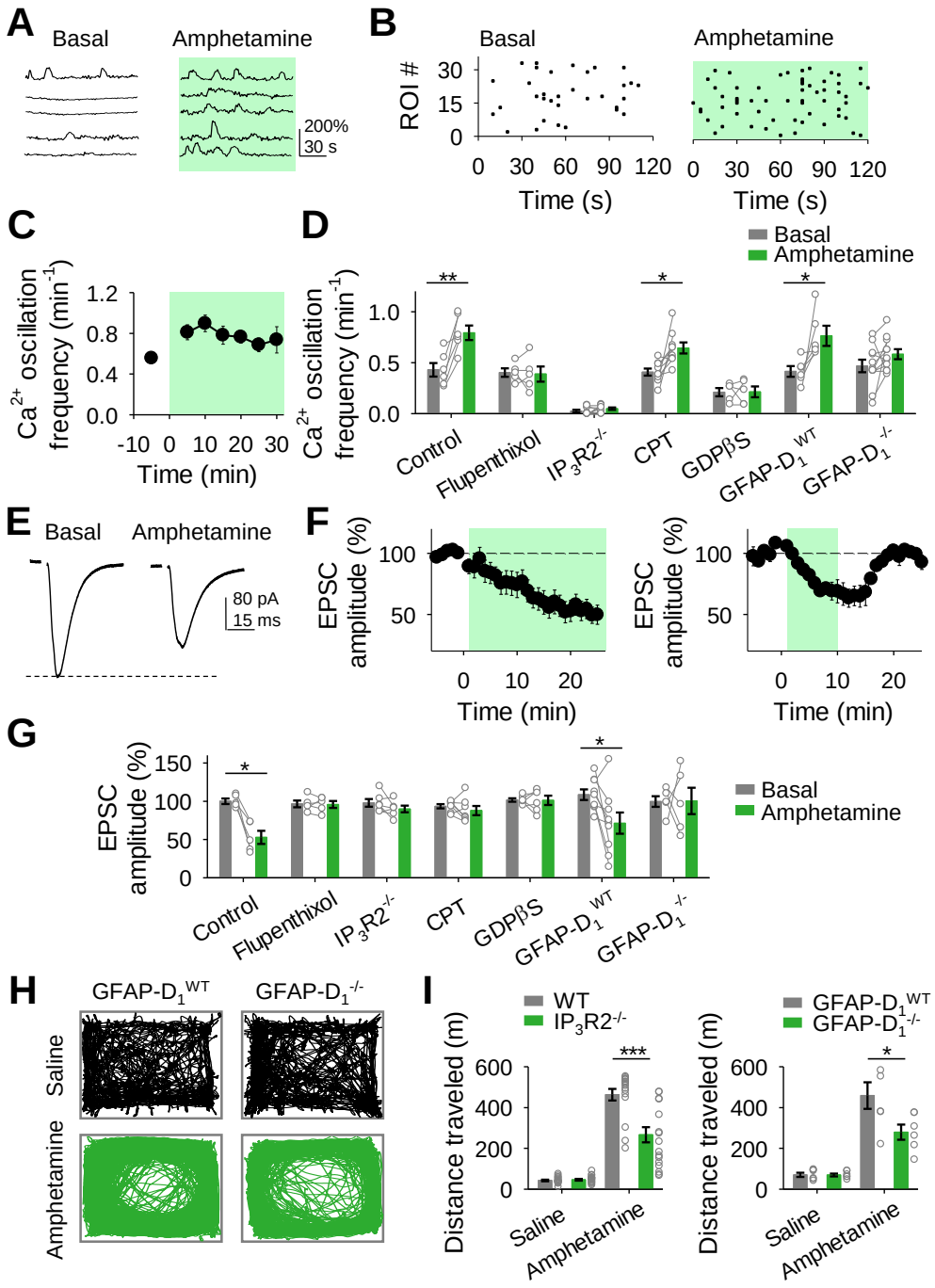
A
Basal
Amphetamine
200%
30 s
B
Basal
Amphetamine
ROI #
30
15
0
0 30 60 90 120
Time (s)
C
Ca2+ oscillation frequency (min-1)
1.2
0.8
0.4
0.0
-10 0 10 20 30
Time (min)
D
Basal
Amphetamine
Ca2+ oscillation frequency (min-1)
1.0
0.5
0.0
**
*
*
Control
Fluperthixol
IP3R2-/-
CPT
GDPβS
GFAP-D1WT
GFAP-D1-/-
E
Basal
Amphetamine
80 pA
15 ms
F
EPSC amplitude (%)
100
50
0 10 20
Time (min)
G
EPSC amplitude (%)
150
100
50
0
*
*
Basal
Amphetamine
Control
Fluperthixol
IP3R2-/-
CPT
GDPβS
GFAP-D1WT
GFAP-D1-/-
H
GFAP-D1WT
GFAP-D1-/-
Saline
Amphetamine
I
WT
IP3R2-/-
Distance traveled (m)
600
400
200
0
***
Saline
Amphetamine
GFAP-D1WT
GFAP-D1-/-
Distance traveled (m)
600
400
200
0
*
Saline
Amphetamine

Figure 7

KEY RESOURCES TABLE

REAGENT or RESOURCE	SOURCE	IDENTIFIER
Antibodies		
Mouse anti-NeuN	Millipore	Cat#: MAB377
Rabbit anti-GFAP	Sigma	Cat#: G9269
Sheep anti-TH	Pel-Freez	P60101-0
Mouse anti-NG2	Millipore	Cat # AB5320.
Rabbit anti-Iba1	Wako	Cat # 019-19741
Guinea pig anti-D1R polyclonal	Frontier Institute co., Japan	GP-Af500; C-terminus 45 aa. of mouse D1R, NM010076
488 donkey anti-sheep	Invitrogen	Ref: A11015
405 goat anti–mouse	Invitrogen	Ref: A31553
488 goat anti-rabbit	Invitrogen	Ref: A11034
Goat anti-guinea pig IgG coupled to 1.4 nm gold	Nanoprobes Inc.	http://www.nanoprobes.com/products/FluoroNanogold.html
Bacterial and Virus Strains		
AAV8-GFAP-hM3D(Gq)-mCherry	UNC vector core	https://www.med.unc.edu/genetherapy/vectorcore/in-stock-aav-vectors/
AAV8-GFAP-mCherry	UMN vector core	http://vvcc.umn.edu/
AAV5-GfaABC1D-PI-LckGCaMP6.SV40	Penn Vector Core	https://gtp.med.upenn.edu/core-laboratories-public/vector-core
AAV5-GfaABC1D-cytoGCaMP6f-SV40	Penn Vector Core	https://gtp.med.upenn.edu/core-laboratories-public/vector-core
AAV8-GFAP-mCherry-CRE	UNC vector core	https://www.med.unc.edu/genetherapy/vectorcore/in-stock-aav-vectors/
AAV5-hSyn-FLEX-ChrimsonR-tdT	UNC vector core	https://www.med.unc.edu/genetherapy/vectorcore/in-stock-aav-vectors/
Biological Samples		

Chemicals, Peptides, and Recombinant Proteins		
Critical Commercial Assays		
Deposited Data		
Experimental Models: Cell Lines		
Experimental Models: Organisms/Strains		
C57BL/6J	The Jackson Laboratory	JAX #000664
$IP_3R2^{-/-}$	Li, X., Zima, A.V., Sheikh, F., Blatter, L.A., and Chen, J. (2005). Endothelin-1-induced arrhythmogenic Ca2+ signaling is abolished in atrial myocytes of inositol-1,4,5-trisphosphate(IP3)-receptor type 2-deficient mice. Circulation research *96*, 1274-1281.	n/a
DrD1 flox/flox	The Jackson Laboratory	JAX #025700
DAT-IRES-CRE	The Jackson Laboratory	JAX #006660

R26-lsl-GCaMP3 mice	The Jackson Laboratory	JAX #014538
GLAST-CreERT2	The Jackson Laboratory	JAX #012586
Oligonucleotides		
Recombinant DNA		
Software and Algorithms		
Clampfit 10.4	Molecular Devices	https://www.moleculardevices.com/
MetaMorph 7.8.8.0	Molecular Devices	https://www.moleculardevices.com/
Fluoview	Olympus	https://www.olympus-lifescience.com/en/
LAS AF Lite	Leica	https://www.leica-microsystems.com/
RZ5P processor	Tucker Davis Technologies	https://www.tdt.com/component/fiber-photometry-rz5p/
ANY-maze	Stoelting Co.	https://www.stoeltingco.com/anymaze.html?gclid=EAIaIQobChMI8avNqv7p5AIViLzACh1YBgfLEAAYASAAEgI3OfD_BwE
SigmaPlot 12.5	Systat Software Inc.	https://systatsoftware.com/products/sigmaplot/sigmaplot-product-updates/
Image J	NIH	https://imagej.nih.gov/ij/
MATLAB	MathWorks	https://www.mathworks.com/products/matlab.html

Other		

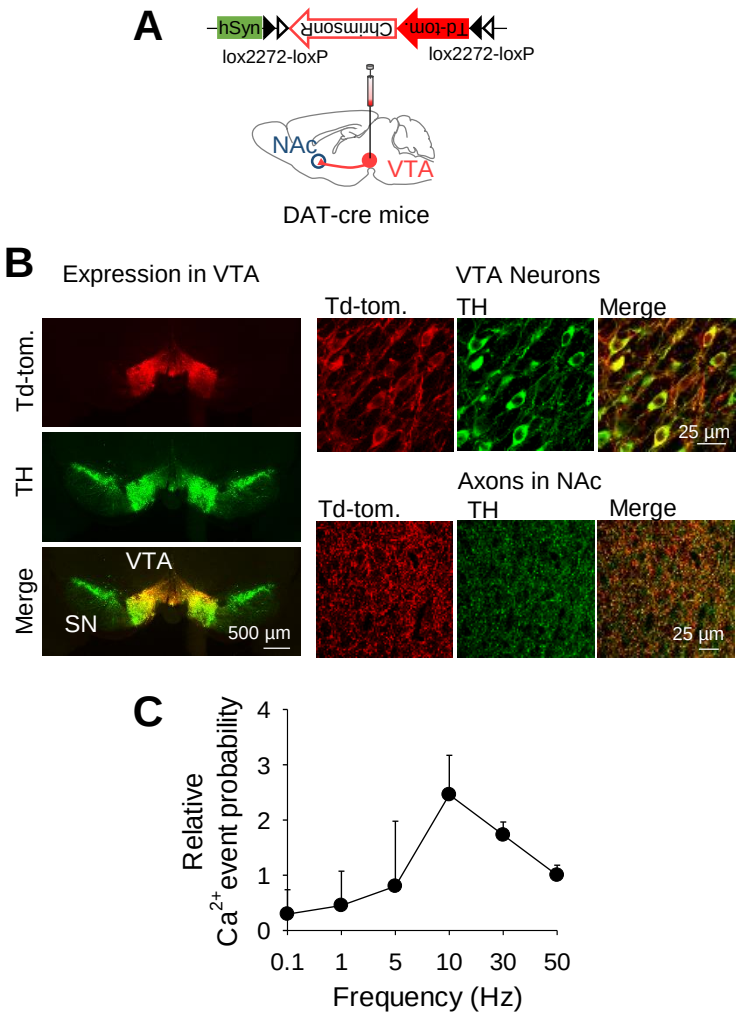

Figure S1. ChrimsonR expression in dopaminergic neurons.
(A) Viral vector injected into the VTA of DAT-cre mice. **(B)** Immunohistochemical images showing expression of AAV5-hSyn-ChrimsonR-TdTomato in neuronal somas in the VTA and axon terminals in the NAc. (**C)** Normalized mean astrocyte responses to different stimulation frequencies.

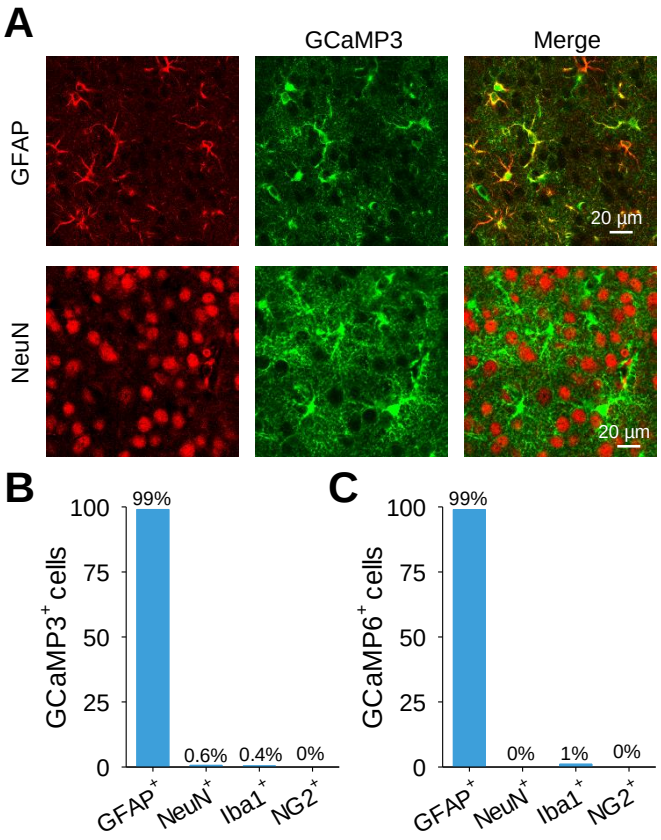

Figure S2. GCaMP expression in astrocytes.
(A) Immunohistochemical images showing expression of GCaMP3 in NAc astrocytes and co-stained with GFAP or NeuN. *From left to right*: cell marker, GCaMP3 and merge. **(B)** Percent distribution of GCaMP3$^+$ cells (n = 511 cells). **(C)** Percent distribution of GCaMP6f$^+$ cells (n = 192 cells).

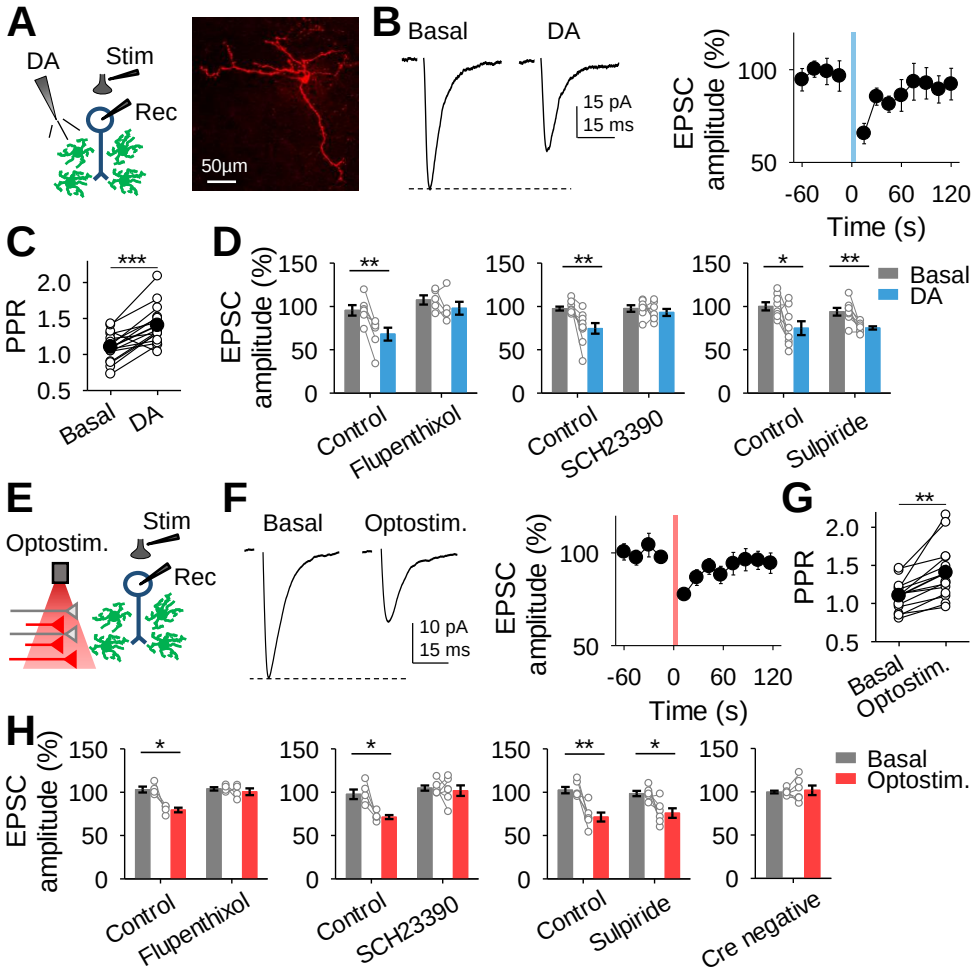

Figure S3. Dopamine depresses excitatory transmission.
(A) Experimental scheme *(right)* and image of a nucleus accumbens medium spiny neuron filled with biocytin through a patch pipette (*left)*. **(B)** Representative EPSC traces before (basal) and after DA application (*right*) and relative EPSC amplitude over time. **(C)** Paired pulse ratio (PPR) before (basal) and after dopamine application. Two-tailed student's paired t-test. **(D)** Relative EPSC amplitude. Two-tailed student's paired t-test. **(E-H)** as a-d, but for optical stimulation. Two-tailed student's paired t-test. Blue and red shadows indicate DA application and optical stimulation, respectively. Data are expressed as mean ± s.e.m., *p<0.05, **p<0.01, ***p<0.001.

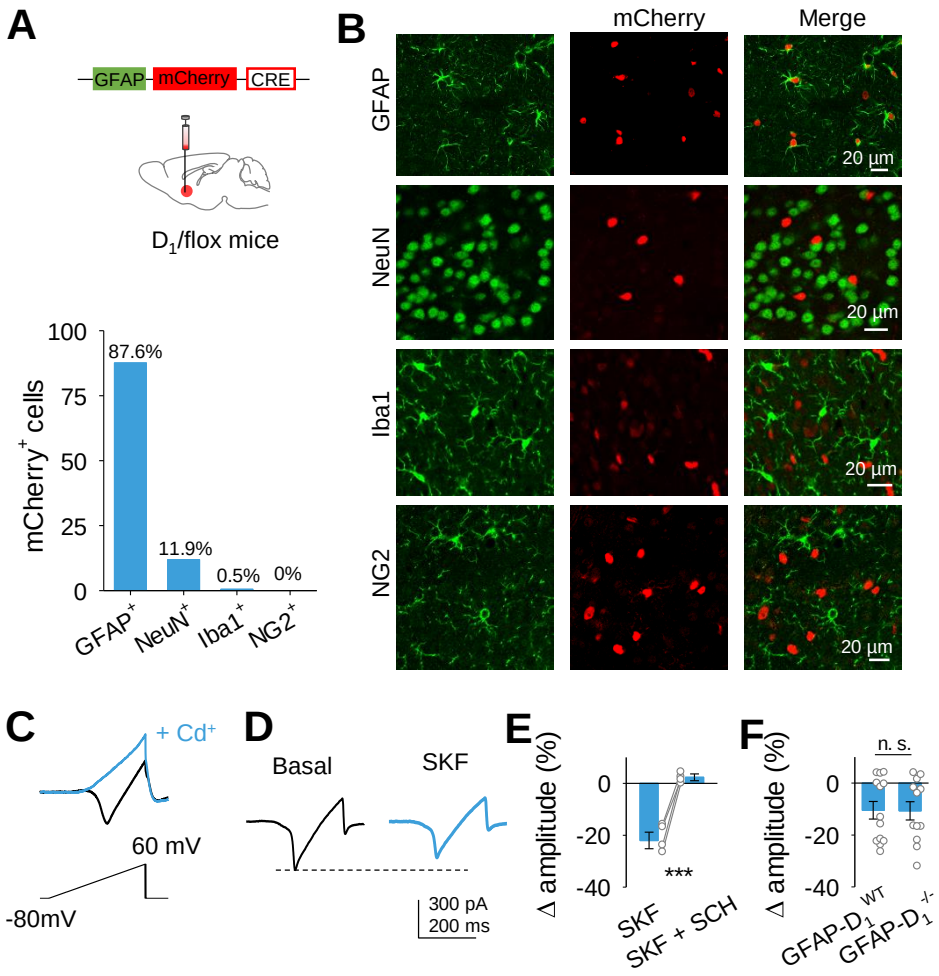

Figure S4. AAV8-GFAP-mCherry-Cre targets astrocytes.
(A) Experimental scheme (*top*) and percent distribution of mCherry⁺ cells (*bottom*). **(B)** Immunohistochemistry images of mCherry⁺ cells co-stained with GFAP, NeuN, Iba1 or NG2 (n = 935 cells). *From left to right:* cell marker, mCherry, and merge. **(C)** Representative Cd⁺ sensitive currents. **(D)** Cd⁺ sensitive current before (basal) and after SKF 38393 application. **(E)** Relative change in amplitude of Cd⁺ sensitive current in SKF 38393 only conditions (SKF) or in SKF 38393 and SCH 23390 conditions (SKF + SCH). Two-tailed student's unpaired t-test. **(F)** Relative change in amplitude of Cd⁺ sensitive current in response to SKF 38393. Data are expressed as mean ± s.e.m., ***p<0.001.

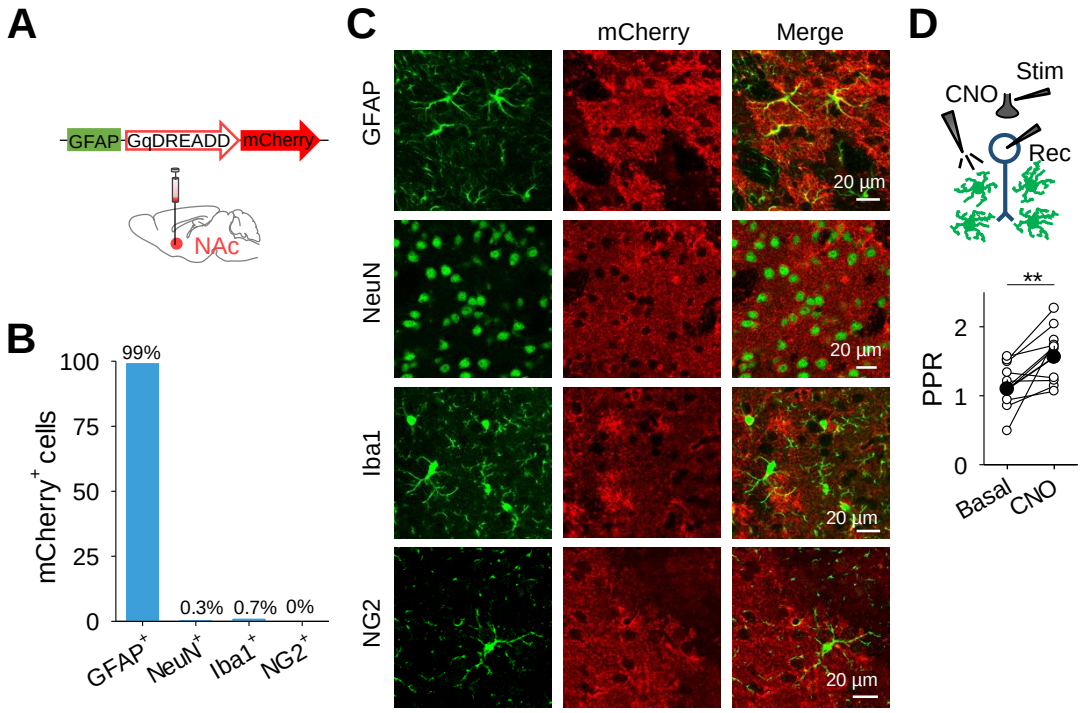

Figure S5: AAV8-GFAP-hM3D(Gq)-mCherry is specifically expressed in astrocytes.
(A) Scheme of experimental approach. **(B)** Percent distribution of mCherry⁺ cells (n = 408 cells). **(C)** Immunohistochemistry images of mCherry⁺ cells co-stained with GFAP, NeuN, Iba1 or NG2. *From left to right:* cell marker, mCherry, and merge. **(D)** Experimental scheme (*top*) and paired pulse ratio (PPR) before (basal) and after CNO application (*bottom*) (n = 10). Two-tailed student's paired t-test. Data are expressed as mean ± s.e.m., **p<0.01.

Kruskal-Wallis One Way ANOVA values					
	H value	DF	P value	Post hoc	q and p values
Fig. 1D	38.085	3	<0.001	Dunn's Method	Control vs Flupenthixol: q=5. 428, p<0.001; Control vs GFP: q=3.502, p<0.001; Control vs Cre negative: q=4.949, p=0.003; Flupenthixol vs GFP: q=0.557, p=1; Flupenthixol vs Cre negative: q=1.114, p=1; GFP vs Cre negative: q=0.23, p=1

Extended data table 1. Full report of Kruskal-Wallis One Way ANOVA values. Full report of H values, degrees of freedom (DF) and p value for the Kruskal-Wallis One Way ANOVA tests performed on non-parametric data and the post hoc analysis q and p values.

One way ANOVA values					
	F value	DF	p value	Post hoc	p values
Fig. 2B	4.539	4	0.004	Fisher LSD Method	Control vs Flupenthixol: p=0.008; Control vs SCH23390: p=0.03; Control vs Sulpiride: p=0.833; Control vs Cocktail: p=0.941
Fig. 2D	10.724	4	<0.001	Fisher LSD Method	Control vs Flupenthixol: p<0.001; Control vs SCH23390: p=0.003; Control vs Sulpiride: p=0.858; Control vs Cre Negative: p=0.005

Extended data table 2. Full report of One way ANOVA values. Full report of F values, degrees of freedom (DF) and p value for the One way ANOVA tests performed and the post hoc analysis p values.

Student's t test				
	Comparison	Condition	Test	t and p values
Fig. 1F	Control vs amphetamine	Fluorescence amplitude (AU)	Two-tailed Student's unpaired t-test	t=-2.48, p=0.017
Fig. 1F	Control vs amphetamine	Rise time (s)	Two-tailed Student's unpaired t-test	t=-3.19, p=0.002
Fig. 1F	Control vs amphetamine	Response width (s)	Two-tailed Student's unpaired t-test	t=-3.19, p=0.026
Fig. 2B	Basal vs DA	Control	Two-tailed Student's paired t-test	t=-4.32, p=0.007
Fig. 2B	Basal vs DA	Flupenthixol	Two-tailed Student's paired t-test	t=-0.81, p=0.811
Fig. 2B	Basal vs DA	SCH23390	Two-tailed Student's paired t-test	t=-0.88, p=0.428
Fig. 2B	Basal vs DA	Sulpiride	Two-tailed Student's paired t-test	t=-7.4, p<0.001
Fig. 2B	Basal vs DA	Cocktail	Two-tailed Student's paired t-test	t=-5.577, p<0.001
Fig. 2D	Basal vs Optostim.	Control	Two-tailed Student's paired t-test	t=-6.22, p<0.001
Fig. 2D	Basal vs Optostim.	Flupenthixol	Two-tailed Student's paired t-test	t=0.139, p=0.892
Fig. 2D	Basal vs Optostim.	SCH23390	Two-tailed Student's paired t-test	t=-0.337, p=0.75

Fig. 2D	Basal vs Optostim.	Sulpiride	Two-tailed Student's paired t-test	t=-7.587, p<0.001
Fig. 2D	Basal vs Optostim.	Cre negative	Two-tailed Student's paired t-test	t=0.645, p=0.554
Fig. 4B	Basal vs DA	Calcium event probability: Control	Two-tailed Student's paired t-test	t=-8.836, p<0.001
Fig. 4B	Basal vs DA	Calcium event probility: GDPβS	Two-tailed Student's paired t-test	t=-0.397, p=0.718
Fig. 4B	Basal vs DA	Calcium event probility: $IP_3R2^{-/-}$	Two-tailed Student's paired t-test	t=-0.312, p=0.76
Fig. 4B	Basal vs DA	EPSC amplitude (%): Control	Two-tailed Student's paired t-test	t=3.731, p=0.007
Fig. 4B	Basal vs DA	EPSC amplitude (%): GDPβS	Two-tailed Student's paired t-test	t=0.152, p=0.885
Fig. 4B	Basal vs DA	EPSC amplitude (%): $IP_3R2^{-/-}$	Two-tailed Student's paired t-test	t=0.188, p=0.856
Fig. 4D	GFAP-D_1^{WT} vs GFAP-$D_1^{-/-}$	Baseline	Two-tailed Student's unpaired t-test	t=3.239, p=0.006
Fig. 4D	Basal vs DA	GFAP-D_1^{WT}	Two-tailed Student's paired t-test	t=-8.725, p<0.001
Fig. 4D	Basal vs DA	GFAP-$D_1^{-/-}$	Two-tailed Student's paired t-test	t=-1.335, p=0.219
Fig. 4D	Basal vs ATP	GFAP-D_1^{WT}	Two-tailed Student's paired t-test	t=-13.502, p<0.001
Fig. 4D	Basal vs ATP	GFAP-$D_1^{-/-}$	Two-tailed Student's paired t-test	t=-21.548, p<0.001
Fig. 4E	Basal vs DA	GFAP-D_1^{WT}	Two-tailed Student's paired t-test	t=10.203, p<0.001
Fig. 4E	Basal vs DA	GFAP-$D_1^{-/-}$	Two-tailed Student's paired t-test	t=1.867, p=0.104
Fig. 5A	Basal vs DA	Control	Two-tailed Student's paired t-test	t=-5.679, p=0.002
Fig. 5A	Basal vs DA	CPT	Two-tailed Student's paired t-test	t=-4.74, p=0.005
Fig. 5A	Basal vs Optostim.	Control	Two-tailed Student's paired t-test	t=-5.425, p<0.001
Fig. 5A	Basal vs Optostim.	CPT	Two-tailed Student's paired t-test	t=-7.752, p=0.001
Fig. 5B	Basal vs DA	Control	Two-tailed Student's paired t-test	t=10.279, p<0.001
Fig. 5B	Basal vs DA	CPT	Two-tailed Student's paired t-test	t=-0.0938, p=0.929
Fig. 5B	Basal vs Optostim.	Control	Two-tailed Student's paired t-test	t=5.474, p=0.002
Fig. 5B	Basal vs Optostim.	CPT	Two-tailed Student's paired t-test	t=-1.451, p=0.197
Fig. 5E	Basal vs DA	Control	Two-tailed Student's paired t-test	t=6.607, p=0.001

Fig. 5E	Basal vs DA	GDPβS	Two-tailed Student's paired t-test	t=0.26, p=0.802
Fig. 5E	Basal vs DA	$IP_3R2^{-/-}$	Two-tailed Student's paired t-test	t=1.804, p=0.121
Fig. 5E	Basal vs Ado	Control	Two-tailed Student's paired t-test	t=4.282, p=0.008
Fig. 5E	Basal vs Ado	GDPβS	Two-tailed Student's paired t-test	t=3.804, p=0.007
Fig. 5E	Basal vs Ado	$IP_3R2^{-/-}$	Two-tailed Student's paired t-test	t=6.753, p<0.001
Fig. 6B	Basal vs CNO	Control	Two-tailed Student's paired t-test	t=-2.965, p=0.041
Fig. 6B	Basal vs CNO	CPT	Two-tailed Student's paired t-test	t=-3.355, p=0.028
Fig. 6B	Basal vs CNO	mCherry	Two-tailed Student's paired t-test	t=-0.474, p=0.656
Fig. 6C	Basal vs CNO	Control	Two-tailed Student's paired t-test	t=3.468, p=0.007
Fig. 6C	Basal vs CNO	CPT	Two-tailed Student's paired t-test	t=-1.244, p=0.260
Fig. 6C	Basal vs CNO	mCherry	Two-tailed Student's paired t-test	t=0.326, p=0.757
Fig. 7D	Basal vs Amphetamine	Control	Two-tailed Student's paired t-test	t=-4.752, p=0.005
Fig. 7D	Basal vs Amphetamine	Flupenthixol	Two-tailed Student's paired t-test	t=-0.242, p=0.821
Fig. 7D	Basal vs Amphetamine	$IP_3R2^{-/-}$	Two-tailed Student's paired t-test	t=-1.484, p=0.176
Fig. 7D	Basal vs Amphetamine	CPT	Two-tailed Student's paired t-test	t=-3.187 , p=0.013
Fig. 7D	Basal vs Amphetamine	GDPβS	Two-tailed Student's paired t-test	t=-0.0473, p=0.962
Fig. 7D	Basal vs Amphetamine	GFAP-D_1^{WT}	Two-tailed Student's paired t-test	t=-2.68, p=0.044
Fig. 7D	Basal vs Amphetamine	GFAP-$D_1^{-/-}$	Two-tailed Student's paired t-test	t=-1.581, p=0.145
Fig. 7G	Basal vs Amphetamine	Control	Two-tailed Student's paired t-test	t=5.444, p=0.006
Fig. 7G	Basal vs Amphetamine	Flupenthixol	Two-tailed Student's paired t-test	t=0.228, p=0.831
Fig. 7G	Basal vs Amphetamine	$IP_3R2^{-/-}$	Two-tailed Student's paired t-test	t=1.509, p=0.192
Fig. 7G	Basal vs Amphetamine	CPT	Two-tailed Student's paired t-test	t=1.036, p=0.34
Fig. 7G	Basal vs Amphetamine	GDPβS	Two-tailed Student's paired t-test	t=0.08, p=0.939
Fig. 7G	Basal vs Amphetamine	GFAP-D_1^{WT}	Two-tailed Student's paired t-test	t=2.824, p=0.022
Fig. 7G	Basal vs Amphetamine	GFAP-$D_1^{-/-}$	Two-tailed Student's paired t-test	t=-0.031, p=0.977

Fig. 7I	WT vs $IP_3R2^{-/-}$	Saline	Two-tailed Student's unpaired t-test	t=-0.796, p=0.432
Fig. 7I	WT vs $IP_3R2^{-/-}$	Amphetamine	Two-tailed Student's unpaired t-test	t=4.604, p<0.001
Fig. 7I	GFAP-D_1^{WT} vs GFAP-$D_1^{-/-}$	Saline	Two-tailed Student's unpaired t-test	t=0.051, p=0.96
Fig. 7I	GFAP-D_1^{WT} vs GFAP-$D_1^{-/-}$	Amphetamine	Two-tailed Student's unpaired t-test	t=2.395, p=0.038
Fig. S3C	Basal vs DA	PPR	Two-tailed Student's paired t-test	t=-4.98, p<0.001
Fig. S3D	Basal vs DA	Control	Two-tailed Student's paired t-test	t=5.23, p=0.003
Fig. S3D	Basal vs DA	Flupenthixol	Two-tailed Student's paired t-test	t=1.348, p=0.249
Fig. S3D	Basal vs DA	Control	Two-tailed Student's paired t-test	t=3.808, p=0.005
Fig. S3D	Basal vs DA	SCH23390	Two-tailed Student's paired t-test	t=0.72, p=0.498
Fig. S3D	Basal vs DA	Control	Two-tailed Student's paired t-test	t=2.743, p=0.029
Fig. S3D	Basal vs DA	Sulpiride	Two-tailed Student's paired t-test	t=4.178, p=0.004
Fig. S3G	Basal vs Optostim.	PPR	Two-tailed Student's paired t-test	t=-4.321, p<0.001
Fig. S3H	Basal vs Optostim.	Control	Two-tailed Student's paired t-test	t=4.081, p=0.027
Fig. S3H	Basal vs Optostim.	Flupenthixol	Two-tailed Student's paired t-test	t=0.599, p=0.591
Fig. S3H	Basal vs Optostim.	Control	Two-tailed Student's paired t-test	t=3.692, p=0.021
Fig. S3H	Basal vs Optostim.	SCH23390	Two-tailed Student's paired t-test	t=0.46, p=0.665
Fig. S3H	Basal vs Optostim.	Control	Two-tailed Student's paired t-test	t=4.44, p=0.007
Fig. S3H	Basal vs Optostim.	Sulpiride	Two-tailed Student's paired t-test	t=2.943, p=0.032
Fig. S3H	Basal vs Optostim.	Cre negative	Two-tailed Student's paired t-test	t= -0.441, p=0.667
Fig. S4E	SKF vs SKF+SCH	Δ amplitude (%)	Two-tailed Student's unpaired t-test	t=-8.209, p<0.001
Fig. S4F	GFAP-D_1^{WT} vs GFAP-$D_1^{-/-}$	Δ amplitude (%)	Two-tailed Student's unpaired t-test	t=-0.046, p=0.964
Fig. S5D	Basal vs CNO	PPR	Two-tailed Student's paired t-test	t=-3.264, p=0.009

Extended data table 3. Full report of Student's t-tests t and p values. Full report of all the Student's t-tests t and p values from main and supplementary figures.

Transgenic mice generation using viral vectors				
			Mouse genotype	**Viral vector**
Mice expressing ChrimsonR in dopaminergic neurons	Fig. 1A-F; Fig. 2C-D; Fig. 3B, Fig. 3E-F; Fig. 5A-B; Fig. S1; Fig. S3E-H;	Control mice: "*Cre negative"*	DAT wild-type littermate mice lacking CRE	AAV5-hSyn-FLEX-ChrimsonR-tdTomato
		Transgenic mice	DAT-IRES-CRE	AAV5-hSyn-FLEX-ChrimsonR-tdTomato
GFAP-D_1 line	Fig. 4C-E; Fig. 6D, 6G-I; Fig. S4	Control mice: "*GFAP-D_1^{WT}"*	DRD1 wild-type littermate mice lacking flox	AAV8-GFAP-mCherry-CRE
		Transgenic mice: "GFAP-$D_1^{-/-}$"	DRD1 flox/flox	AAV8-GFAP-mCherry-CRE
Mice expressing DREADDs in astrocytes	Fig. 6A-C; Fig. S5	Control mice: "*mCherry"*	C57BL/6J	AAV8-GFAP -mCherry
		Transgenic mice	C57BL/6J	AAV8-GFAP-Gq-DREADD-mCherry

Extended data table 4. Report of mice genotype and viral vectors used for generating transgenic mice. Report of the mice genotype and the viral vectors used to generate experimental transgenic mice and their respective control mice in main figures and supplementary figures.